NAR Cancer, 2025, **7**, zcaf057
https://doi.org/10.1093/narcan/zcaf057
DNA Damage Sensing and Repair

OXFORD

Replication-associated base excision repair/single-strand break repair regulates PARG inhibitor response via the PRMT1/PRMT5/ATR axis

Md Ibrahim [1,2], Wynand P. Roos [3], Jacob C. Schwartz[3], Md Maruf Khan[3], Rasha Q. Al-Rahahleh[3], Libby A. Beers[3], Charlotte R. Pearson[3], Kahrie T. Langham[3], Louis Boyang[3], Jennifer Clark[1], Faisal Hayat[1], Qingming Fang[1,4], Christopher A. Koczor[1], Marie E. Migaud[1], Robert W. Sobol [1,3,*]

[1]Department of Pharmacology & Mitchell Cancer Institute, University of South Alabama, Mobile, AL 36604, United States
[2]Present address: Department of Pharmaceutical and Biomedical Sciences, College of Pharmacy, California Northstate University, Elk Grove, CA 95757, United States
[3]Department of Pathology and Laboratory Medicine, Warren Alpert Medical School & Legorreta Cancer Center, Brown University, Providence, RI 02912, United States
[4]Present address: Department of Biochemistry and Structural Biology, Greehey Children's Cancer Research, UTHSCSA, San Antonio, TX 78229, United States

*To whom correspondence should be addressed. Email: robert_sobol@brown.edu

Abstract

Poly(ADP-ribose) polymerases 1 and 2 (PARP1/PARP2), and poly(ADP-ribose) glycohydrolase (PARG), modulate the level of poly(ADP-ribose) (PAR), a post-translational protein modification, in response to DNA damage or replication stress. Here, we find that replication-dependent and PARP1/PARP2-mediated PARylation recruits the base excision repair (BER)/single-strand break repair (SSBR) scaffold protein XRCC1 and the associated factors DNA polymerase β (POLB), aprataxin (APTX), and DNA ligase isoform 3 (LIG3). Further, these BER/SSBR proteins promote resistance to inhibitors of PARP1/PARP2 and PARG, as loss of these proteins sensitizes glioblastoma and ovarian cancer cells to each. In addition, depletion of these replication-associated BER/SSBR factors leads to enhanced PAR levels and PARG inhibitor-induced activation of the ATR/CHK1 S-phase checkpoint kinases. Both PARG inhibition and ATR inhibition lead to elevated ATM- and DNA-PK-dependent KAP1 phosphorylation. In turn, inhibition of either ATR or CHK1 enhances the cellular response to PARG inhibitors. Finally, inhibition of the ATR regulators PRMT1 or PRMT5 synergizes with PARG inhibition, implicating replication-associated BER/SSBR and PARylation in the activation of the PRMT1/PRMT5/ATR axis. This study highlights the role of BER/SSBR in protecting the cell during S-phase to suppress PARylation-induced checkpoint activation, which may suggest a potential intervention strategy for PARG inhibitor-resistant tumors.

Graphical abstract

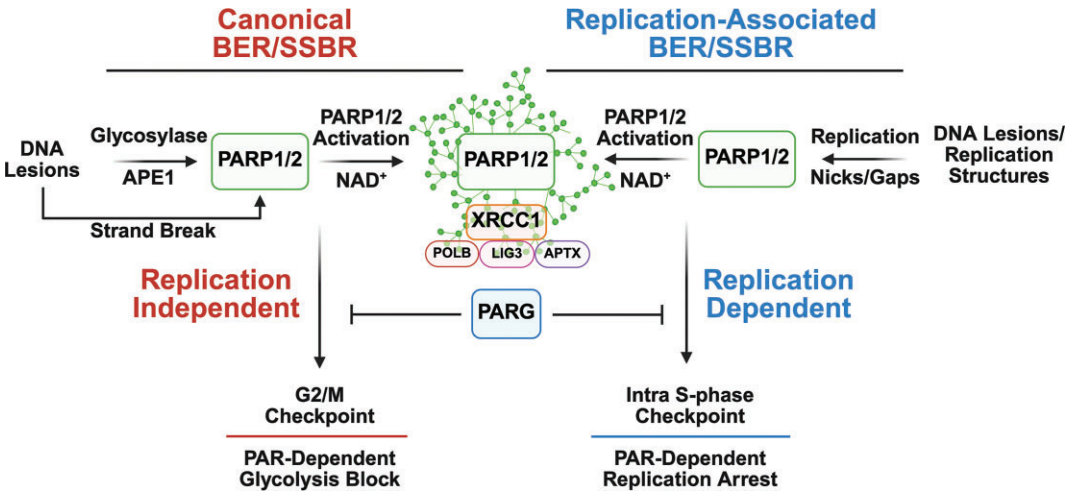

Received: August 19, 2025. **Revised:** December 10, 2025. **Accepted:** December 10, 2025

Introduction

Protein mono-ADP-ribosylation (MARylation) and poly-ADP-ribosylation (PARylation) are post-translational modifications catalyzed by the ADP-ribose polymerase family of enzymes [1–4]. MARylation is the transfer of one ADP-ribose unit, whereas PARylation involves the successive transfer of multiple ADP-ribose units, poly(ADP-ribose) (PAR), to specific residues within target proteins [1, 5]. There are 17 proteins in the PARP family of enzymes [1], yet only PARP1, PARP2, PARP5a, and PARP5b catalyze the formation of PAR chains [6, 7]. Of these, only PARP1 and PARP2 synthesize PAR in response to DNA breaks [1], which in turn facilitates the regulation of the DNA damage response (DDR) and impacts chromatin reorganization, transcription, mitosis, and cell death [8–10].

PAR plays a critical role in DNA repair by acting as a signaling platform to promote the recruitment of DNA repair factors as mediated via their PAR-binding domains (PBDs) [8, 11–15] to sites of DNA damage to promote, primarily, base excision repair (BER) and single-strand break repair (SSBR) [8, 13]. Other DNA repair pathway proteins shown to be regulated by PARP1/PARP2 activation include MutSα and mismatch repair (MMR) [16], UV damage repair via DDB2/XPC and nucleotide excision repair (NER) [17, 18], and DNA polymerase theta (Pol θ)-mediated end-joining (TMEJ) [19].

The involvement of PARP1 and PARP2 in BER and SSBR has been well documented [13, 20–22]. As we and many others have shown, the formation of a DNA single-strand break, whether mediated by a bifunctional DNA glycosylase to initiate BER, by the endonuclease APE1 during BER, or directly from DNA damage to initiate SSBR, gives rise to PARP1/PARP2 activation [2, 20]. The model for the canonical BER mechanism suggests that APE1 binds to and hydrolyzes apurinic or apyrimidinic (AP) sites in DNA [23], forming the DNA break that activates PARP1/PARP2, highlighting a functional relationship between APE1 and PARP1 [24, 25]. In short, canonical BER and SSBR respond to base damage or single-strand DNA breaks (SSBs) in all phases of the cell cycle, followed by PARP1/PARP2 activation [2, 20, 22, 26, 27]. Once activated, PARylation facilitates recruitment of the scaffold protein XRCC1 and the end- and gap-processing BER/SSBR proteins POLB, APTX, APLF, PNKP, and LIG3 [8, 13]. The recruitment of these BER/SSBR proteins to sites of DNA damage is PARP1- and PARP2-dependent, and some (POLB, APTX, LIG3) are also XRCC1-dependent [8, 13, 28, 29]. There is a reciprocal relationship between PARP1, PARP2, XRCC1, and POLB since loss of either XRCC1 or POLB delays release of PARP1 from sites of DNA damage, whereas PARP2 release is only dependent on XRCC1 [13]. Conversely, the release of the BER proteins XRCC1, POLB, APTX, and LIG3 from DNA damage sites is regulated by both PAR and NAD^+ levels [2, 13]. Once repair is complete, the removal of the damage signal (PAR) is mediated by the PAR-degrading enzymes PARG, TARG1, and ARH3 [2, 20]. Of note, the inhibition of PARG, but not TARG1, attenuates the release of these BER factors from sites of DNA damage, blocking the completion of BER and promoting persistent PAR levels and PAR signaling [30–32].

Replication stress and the activation of the DDR are hallmarks of the cancer phenotype [33–35], highlighting numerous potential cancer-specific targets that may be exploited for selective therapy approaches. Replication stress results from DNA lesions and unusual DNA structures (hairpins, triplexes, G-quadruplexes) encountered by the replication fork [36, 37], as well as from oncogene activation or tumor suppressor gene inactivation [38]. Further, replication stress may result from defects in the nucleotide pool or altered expression of replication machinery proteins [39], from head-on collisions with the transcription machinery and the resulting accumulation of R-loops [40, 41], as well as DNA single-stranded gaps due to defects in Okazaki fragment processing [42] or BRCA1/2 expression and function [43, 44]. In this regard, activation of PARP1/PARP2 and the resulting synthesis of PAR play a critical role in the DDR in response to stalled replication forks [31, 45–57], R-loops [58], single-stranded DNA gaps [44, 46, 59, 60], DNA damage at telomeres [61–63], and G-quadruplexes [63–65], among other genome disturbances, such as DNA strand breaks formed during ribonucleotide excision repair (RER) [66] or by unligated Okazaki fragments [67].

The role of PARP1/PARP2 in protecting cells from DNA damage at the replication fork is exploited in homologous recombination (HR)-deficient (BRCA1 or BRCA2) tumors, as loss of BRCA1 or BRCA2, due to mutational inactivation, causes a synthetic lethal interaction with PARP inhibitors (PARPi) [68, 69]. Conversely, PARG interacts with PCNA at the replication fork to counteract prolonged replication stress [31, 55, 70, 71]. PARG inhibitors (PARGi) cause accumulation of PAR at the replication fork [31, 67], slow down fork progression, cause the accumulation of single-stranded DNA gaps, suppress fork restart by perturbing RECQ1 helicase activity, and induce the activation of the ATR/CHK1 S-phase checkpoint [31, 46, 54, 55, 72–75]. Despite demonstrated efficacy in some cell lines, PARG inhibition was shown to be minimally responsive in numerous patient-derived ovarian cancer cells and cell lines [74, 76], as well as in glioma cell lines, glioma stem cells (GSCs), and head and neck cancer cells, among others [30, 31, 75, 77]. More recently, we have shown that defects in XRCC1, FEN1, or POLB expression or activity lead to elevated levels of PAR in replicating GSCs, glioma cells, ovarian cancer cells, and head & neck cancer cells, leading to activation of the PAR-induced S-phase checkpoint [30, 31, 75, 77, 78].

These earlier studies formed the basis for this study, where we demonstrate that XRCC1, POLB, APTX, and LIG3, but not APE1, regulate the activation of PARP1/PARP2 during replication, in what may be called replication-associated BER/SSBR. These BER and SSBR factors each regulate the cellular response to PARP inhibitors, further documenting a role for these proteins in suppressing the activation and cellular dependence on PARP1/PARP2. In addition, we show that these BER/SSBR proteins regulate the level of replication-dependent PAR levels and, in turn, suppress the cellular response to PARG inhibition, likely blocking the accumulation of replication-induced single-strand DNA gaps that have been suggested to modulate PARG inhibitor efficacy [46]. We show that modulation of replication-stress-mediated PAR levels, in response to PARG inhibition, leads to hyperactivation of the S-phase checkpoint that implicates the ATR/CHK1 signaling node [8] and ultimately replication catastrophe as revealed by elevated KAP1 phosphorylation. Further, we find that Protein Arginine Methyltransferase (PRMT) [79] isoforms 1 and 5, reported to catalyze asymmetric (PRMT1) and symmetric (PRMT5) dimethyl substitutions at arginine residues, and targets ATR [80–82], synergize with PARG inhibitors.

Overall, we suggest that these studies implicate replication-associated BER/SSBR and PARylation in the activation of the PRMT1/PRMT5/ATR axis and highlight the crucial role of replication-associated BER/SSBR in protecting the cell during S-phase to suppress PARylation-induced checkpoint activation and replication catastrophe.

Materials and methods

All reagents, including antibodies, inhibitors, cell lines, oligonucleotides/gRNAs, recombinant DNA, software, and algorithms, used in this study are listed in Supplementary Table S1, including catalog # and source.

Chemicals and reagents

The NAD^+ precursor NRH (dihydronicotinamide riboside; 1-[(2R,3R,4S,5R)-3,4-dihydroxy-5-(hydroxymethyl)tetrahydrofuran-2-yl]-4H-pyridine-3-carboxamide) was prepared as described [83]. Briefly, powdered NRH was dissolved in molecular-grade sterile water to prepare a stock solution of 100 mM. Thymidine was freshly prepared as a 10 mM solution in PBS just before use. PARG inhibitor (PDD00017273), ATR inhibitor (Ceralasertib, AZD6738), ATM inhibitor (KU-55933), CHK1 inhibitor (MK8776), DNA-PK inhibitor (KU-57788), PRMT1 inhibitor (GSK3368715), PRMT5 inhibitor (PRT543), and PARP1/PARP2 inhibitors BMN-673, ABT-888, AG014699, MK-4827, and AZD2281, were kept as 10 mM DMSO stocks. All stock solutions were stored at −80°C.

Cell lines

The LN428 cell line is a human glioblastoma-derived cell line with mutations in the *TP53* gene and deletions in the p14ARF and p16 genes, as previously described [84]. PE01 and C4-2 cell lines were generous gifts from Dr Sharon Cantor (University of Massachusetts, USA) and Dr Toshiyasu Taniguchi (Tokai University School of Medicine, Japan), respectively [85, 86]. The BRCA2-deficient PE01 cell line was derived from an ovarian cancer patient. The BRCA2-proficient "revertant" C4-2 cell line was derived from PE01 and acquired resistance to both cisplatin and PARPi due to a secondary mutation restoring BRCA2 function [85, 86]. ES-2 is an ovarian clear-cell carcinoma cell line. 293-FT cells were derived from human embryonic kidney cells transformed with the SV40 large T antigen. RPE-1 cells are hTERT-immortalized retinal pigment epithelial cells [87]. Cell lines were routinely validated by Genetica Cell Line Testing. Mycoplasma contamination was monitored bimonthly using Lonza MycoAlert®. Cells at passage number 15 or lower were used for all experiments.

LN428, LN428/PARP2-KO, LN428/PARP1-KO/PARP2-KO, LN428/POLB-KO, LN428/APTX-KO, LN428/LIG3-KO, LN428/LivePAR, and LN428/XRCC1-KO/LivePAR cells were cultured in MEM Alpha supplemented with 10% heat-inactivated (HI) fetal bovine serum (FBS), L-glutamine, and Antibiotic-Antimycotic. LN428/PARP1-KO and LN428/XRCC1-KO cells were additionally supplemented with puromycin (1 μg/ml). LN428/PARP1–XRCC1/Split-TurboID cells were supplemented with both hygromycin (200 μg/ml) and puromycin (1 μg/ml). During experiments, hygromycin and/or puromycin were omitted. ES-2, ES-2/XRCC1-KO, ES-2/POLB-KO, ES-2/APTX-KO, ES-2/LIG3-KO, PEO1, C4-2, C4-2/XRCC1-KO, C4-2/POLB-KO, C4-2/APTX-KO, and C4-2/LIG3-KO cells were cultured in RPMI supplemented with 10% HI FBS, L-glutamine, and penicillin-streptomycin. ES-2/PARP1–XRCC1/Split-TurboID cells were additionally supplemented with puromycin (1 μg/ml). RPE-1, RPE-1/APE1-KO, and RPE-1/XRCC1-KO cells were cultivated in DMEM/F12 supplemented with GlutaMAX and 10% HI FBS. All cells were cultured in a humidified incubator at 37°C with 5% CO_2.

Transfection, lentivirus production, and cell transduction

Transfection

ES-2/PARP1–XRCC1/Split-TurboID cells were created by transfecting the pLV-Puro-EF1A-HA-PARP1-3xGS-TurboC-T2A-XRCC1-myc-3xGS-TurboN construct into ES-2 cells using polyethylenimine hydrochloride (PEI) (#24765; Polysciences), and stable clones were selected using puromycin. Plasmid DNA (1 μg) was mixed with 4 μg PEI in 1 ml serum and antibiotic-free media. Following 30 min incubation, the DNA/PEI complex was added to 80% confluent ES-2 cells in a 60 mm Petri dish, dropwise. Following 8 h of incubation, the medium was changed, and selection for stable clones started 48 h later in media supplemented with puromycin (1 μg/ml).

Virus production

293-FT cells were used to generate lentivirus expressing Cas9/sgRNA, LivePAR, or the Split-TurboID expression vectors. Cells (1×10^6 cells/dish) were seeded onto a 60 mm petri dish and allowed to grow overnight. Packaging vectors pMDLg/pRRE, pRSV-Rev, and pMD2.G, and the shuttle/transfer vector were co-transfected into 293-FT cells using the TransIT-X2 Dynamic Delivery System. The supernatant containing the lentivirus was collected 48 h later and filtered using 0.45 μm filters to remove cell debris and isolate the viral particles, as described previously [13, 31].

Transduction

Target cells (2×10^5 cells/well) were seeded onto a six-well plate and incubated for 24 h. The media was replaced with 1 ml of media containing polybrene (2 μg/ml), followed by dropwise addition of the lentiviral particle solution (1 ml). After overnight incubation at 32°C, the lentivirus-containing media was replaced with fresh media, and the cells were allowed to grow for 48 h before adding selection media.

Lentiviral-mediated knockout of *PARP1* and *XRCC1* by CRISPR/Cas9 in LN428 cells

A lentiviral vector derived from pLentiCRISPRv2, expressing Cas9 and either a PARP1 guide RNA (gRNA) targeting exon 1 or an XRCC1 gRNA targeting exon 3, was generously provided by Dr Wim Vermeulen (Erasmus MC, Netherlands) [13, 88]. Lentiviruses were prepared, and LN428 cells were transduced as previously described [13, 31]. Following overnight transduction with either the PARP1-KO or XRCC1-KO gRNA virus, the media were replaced with fresh media, and cells were allowed to propagate to confluence. Cells were then subjected to puromycin selection (1 μg/ml) for 2 weeks. Knockout validation was performed by immunoblotting, using a PARP1 antibody for PARP1-KO cells and an XRCC1 antibody for XRCC1-KO cells. H3 protein expression served as the loading control.

Non-viral-mediated knockout of *PARP2*, *XRCC1*, *POLB*, *APTX*, or *LIG3* in LN428, ES-2, or C4-2 cells

PARP2 was knocked out in LN428 and LN428/PARP1-KO cells; *XRCC1* in ES-2 and C4-2 cells; *POLB* in LN428, ES-2, and C4-2 cells; *APTX* in LN428, ES-2, and C4-2 cells; and *LIG3* in LN428, ES-2, and C4-2 cells. Cells were seeded at a density of 2×10^5 cells/well in a six-well plate and incubated for 24 h. The non-viral ribonucleoprotein (RNP) transfection complex, purchased from Synthego Corporation, was prepared by combining three single guide RNAs (sgRNAs) targeting an early exon of each respective gene—*PARP2*, *XRCC1*, *POLB*, *APTX*, or *LIG3*—with purified Cas9 protein and the CRISPRMAX-Cas9 transfection reagent in serum-free Opti-MEM. Transfection complexes were incubated for 30 min before dropwise addition to the cells. Two to three days later, the medium containing the transfection reagent was replaced with fresh medium, and the cells were allowed to propagate to confluence. Knockout validation was confirmed by immunoblot analysis of whole-cell lysates, compared to a non-targeted control. The following antibodies were used: anti-PARP2, anti-XRCC1, anti-POLB, anti-APTX, and anti-LIG3. H3 was used as a loading control.

Cell protein lysate preparation

Protein extracts were prepared from parental and genetically modified human cancer cells using 2× clear Laemmli buffer (2% SDS, 20% glycerol, 62.5 mM Tris–HCl, pH 6.8) as previously described [13, 31, 89]. Generally, an equal number of cells ($2–3 \times 10^5$) were seeded in six-well plates and allowed to reach 60%–80% confluency after 24 h of culture. Following treatment with varying times and concentrations (as indicated in the figures), the treatment medium was removed, and the cells were washed twice with PBS. Subsequently, 100–200 μl of 2× clear Laemmli buffer was added, the cells were scraped using a cell scraper, and the lysate was transferred to a 1.5 ml Eppendorf tube, followed by heating to 95°C for 5 min. Protein concentrations were determined using a NanoDrop 2000c Spectrophotometer [90].

Immunoblot

Equal amounts of whole-cell lysate (30–50 μg protein) were loaded into each well of Novex 4%–12% Bis-Tris gels and subjected to electrophoresis at 100–120 V for 1.5 h. Proteins were separated by sodium dodecyl sulfate–polyacrylamide gel electrophoresis (SDS–PAGE) and transferred to mini-nitrocellulose membranes (0.2 μm) using the Trans-Blot Turbo transfer system (Bio-Rad) for 18 min. Membranes were blocked with 5% blotting-grade non-fat milk powder in Tris-buffered saline containing 0.1% Tween 20 (TBST) for 1 h at room temperature. Following blocking, membranes were probed overnight with primary antibodies (as indicated in the figure legends), followed by three 10-min washes in TBST. Subsequently, membranes were probed with a secondary antibody (goat anti-mouse/rabbit-HRP conjugated). The protein bands were then detected using Clarity Western ECL Substrate. To determine the induction factors (I.F.) of pCHK1 (S345) and pCHK1 (S317) upon PARG and/or ATR, ATM, and DNA-PK inhibition (as shown in Fig. 6A), a densitometry analysis of the immunoblots was performed using ImageJ. First, the relative amounts of H3 were determined to account for differences in loading. Then, taking into account these differences, the relative amounts of pCHK1 (S345) and pCHK1 (S317) in the treated samples were expressed as a factor compared to the control.

Cell cycle synchronization

Double thymidine block

To synchronize ES-2 cells at the G1/S-phase border, the double thymidine block approach was used [91]. Briefly, cells were seeded at a density of 1×10^6 cells in a 100 mm dish and incubated for 24 h. Cells were then treated with 2 mM thymidine for 24 h, followed by release into fresh medium for 8 h. Subsequently, cells were re-treated with 2 mM thymidine for an additional 24 h. The arrested/synchronized cells (with no DNA replication) were then released into fresh medium for 0 (no replication), 2, 4, 6, or 8 h. Cell cycle analysis was performed on both the thymidine-arrested and released groups to confirm the degree of synchronization. Following confirmation of proper synchronization in the G1-phase of the cell cycle (non-replicating) or release into the S-phase of the cell cycle (replicating), a PAR assay was performed for each condition to determine the level of PAR in resting versus replicating cells.

Serum starvation

To synchronize LN428 or the LN428/PARP1–XRCC1/Split-TurboID cells at the G1/S-phase border, serum starvation [92] was employed, followed by release into the S-phase of the cell cycle. Serum-free media was used to seed $1–1.5 \times 10^6$ cells onto 100 mm or 150 mm dishes and incubated for 24 h. One group of cells (released from serum starvation, replicating) was then released into serum-enriched fresh media for the times indicated in the figure legends (replicating). Another group of cells (continuously serum-starved, non-replicating) was maintained in serum-free media for up to 24 h. Cell cycle analysis was performed on both groups using either Hoechst staining with the Nexcelom Celigo Imaging Cytometer (Perkin Elmer) or PI staining by flow cytometry. Following confirmation of proper synchronization into the G1-phase of the cell cycle (non-replicating) or S-phase of the cell cycle (replicating), the PAR assay and Split-TurboID experiments were performed.

CDK4/6 inhibition

To synchronize ES-2/PARP1–XRCC1/Split-TurboID cells in G1, the CDK4/6 inhibitor (CDK4/6i) ribociclib was used [93]. Cells were exposed to 2 μM CDK4/6i for 48 h. Cells were then released from the G1 arrest and allowed to enter S-phase by media change, or not, for 6 h. During these 6 h, cells were exposed to 10 μM PARGi and 100 μM NRH. One hour before the end of the 6 h, 100 μM biotin was added to the cells.

PAR analysis by immunoblot

To analyze replication-dependent PAR synthesis, parental and BER/SSBR-modified cells were treated with vehicle (DMSO), the NAD^+ precursor NRH (100 μM), the PARG inhibitor PDD00017273 (10 μM), or the combination of NRH and PARGi (same doses) for the times indicated in the figures. Following treatment, cells were washed twice with PBS, trypsinized, and equal numbers of cells (3×10^6) from each treatment condition were processed for lysate preparation using 2× clear Laemmli buffer (2% SDS, 20% glycerol, 62.5 mM Tris–HCl, pH 6.8), a buffer optimal for preparing cell

lysates for PAR analysis. The immunoblot was then performed as described.

Immunofluorescence

Colocalization of PAR and pRPA(S4/S8) foci was quantified by confocal microscopy, as previously described [94]. Shortly, LN428/LivePAR and LN428/XRCC1-KO/LivePAR cells were plated onto microscope coverslips in 60 mm Petri dishes. Before use, the coverslips were prepared by first washing them in diethyl ether, then in decreasing concentrations of ethanol, then in 1N HCl, and finally in ddH_2O. Two days after plating, the cells were exposed to 10 μM PARGi and 100 μM NRH for 8 h. Following exposure, the cells were first prefixed in 4% formaldehyde in PBS (15 min, room temperature) and then in methanol:acetone (7:3, 9 min, −20°C). The first antibody [anti-pRPA(S4/S8)] was added overnight (4°C), and the second antibody was added for 2–3 h at room temperature. The coverslips were mounted onto glass slides in Vectashield (H-1000) containing DAPI. The fluorescence signals for EGFP (LivePAR), Alexa Fluor® 568 [pRPA(S4/S8)], and DAPI (DNA) were detected, imaged, and quantified using a Nikon Ti2-E inverted confocal microscope at a 63× (N. A. 1.42) magnification. The microscope is equipped with Ax-R and Ax-R 2k Resonant + Galvo Scan Head. Foci were scored in the ImageJ software.

Caspase-3/7 activity assay

To measure Caspase-3/7 activity in response to PARGi treatment, LN428 and the corresponding BER/SSBR-KO cells were seeded in a 96-well plate (5000 cells/well) and incubated overnight. Both WT and BER/SSBR-KO cells were treated with PARGi (10 μM) for 24, 48, and 72 h. For Caspase-3/7 activation analysis, a mixture of ViaStain Live Caspase-3/7 substrate (2 μM) and Hoechst 33342 (2 μM) was added to both control and treated wells without removing preconditioned media. The plates were then incubated at 37°C for 1 h. Caspase-3/7 activity was determined using a Celigo S Image Cytometer (Nexcelom Bioscience, Perkin Elmer) by capturing the Caspase-3/7 signal (green, excitation/emission wavelength: 490 nm/520 nm) merged with the nuclear signal (blue, excitation/emission wavelength: 377 nm/470 nm). The total number of cells exhibiting Caspase-3/7 positivity was quantified on 2D scatter plots (green intensity versus blue intensity) using the built-in gating interface of the Celigo S Image Cytometer, as described [95].

Cell cycle analysis

Cell synchronization in the G1 phase of the cell cycle and release into the S phase of the cell cycle were determined by flow cytometric analysis. Both serum-starved/thymidine-arrested and released cells were trypsinized, centrifuged, and washed twice with ice-cold PBS. An equal number of cells (1×10^6) from each condition were fixed overnight with 70% ethanol at −30°C. The cells were then washed twice with PBS and resuspended in 0.5 ml FxCycle™ PI/RNase staining solution and incubated for 30 min at room temperature. Flow cytometry was used to determine DNA content (FACS Canto II, BD Biosciences, San Jose, CA). Modfit LT Software V4.1 was used to generate a cell cycle distribution model. Alternatively, cell cycle analysis was performed using Hoechst staining with the Nexcelom Celigo Imaging Cytometer (Perkin Elmer).

Cell viability assay

Cell viability in response to drug treatment (PARPi, PARGi, ATRi, ATRi + PARGi, CHKi, CHKi + PARGi, PRMT1i, PRMT5i, PRMT1i + PARGi, and PRMT5i + PARGi) was determined as described [75]. Shortly, cells were seeded onto a 96-well plate (800 cells/well). After 24 h of incubation, cells were treated with a single or combined dose (multiple dilutions as indicated in the figures) without removing preconditioned media. After 120 h (5 days), total and dead cells were stained with Hoechst 33342 (2 μM) and Propidium Iodide (1.5 μM), respectively, followed by 15 min of incubation at 37°C. Total and dead cells were counted using a Celigo S Image Cytometer (Nexcelom Bioscience, Perkin Elmer) by capturing the Hoechst dye signal (excitation/emission wavelength for the blue channel: 377 nm/470 nm) and the PI signal (excitation/emission wavelength for the red channel: 531 nm/629 nm).

Split-TurboID experiments for determining PARP1/XRCC1 interacting partners

To label transient and stable interacting proteins in proximity of the PARP1/XRCC1 complex that forms in response to DNA damage, we employed a Split-TurboID approach [31, 96]. For this approach, the biotinylation protein TurboID was split into an N-terminal domain (N-TurboID) and a C-terminal domain (C-TurboID) [96]. The N-TurboID domain was fused in-frame to the C-terminus of XRCC1 to create the plasmid pLV-Puro-EF1A-XRCC1-Myc-4GS-TurboN, also encoding the gene for puromycin selection. The C-TurboID domain was fused in-frame to the C-terminus of PARP1 to create the plasmid pLV-Hygro-EF1A-3xHA-PARP1-4GS-TurboC, also encoding the gene for hygromycin selection. These plasmids were designed in-house and obtained from VectorBuilder. PARP1/Split-TurboID and XRCC1/Split-TurboID lentiviruses were prepared as described, and LN428 cells were transduced with each separately. Expression of both fusion proteins was confirmed by immunoblot, and cells were maintained with concurrent treatment with hygromycin and puromycin.

Using this Split-TurboID method, PARP1/XRCC1 interacting proteins were determined under replicating versus non-replicating conditions. LN428/PARP1–XRCC1/Split-TurboID cells were subjected to serum starvation as described above to create replicating and non-replicating cell groups before biotin labeling. Cells (5×10^6) were seeded onto a 150 mm dish, and after 24 h of incubation, the medium was supplemented with DMSO (control) or biotin (100 μM) for 1 h (two plates for each group). Biotinylation was halted by placing the cell plates on ice, followed by a wash with ice-cold PBS. Cells were harvested with a cell scraper, then lysed with an equal volume of lysis buffer [1% SDS, 10 mM ethylenediaminetetraacetic acid (EDTA), pH 8.0, 50 mM Tris–HCl, pH 8.0, protease inhibitors]. Protein lysates were quantified using the NanoDrop 2000c Spectrophotometer [90]. An equal quantity of proteins was incubated overnight with Streptavidin Mag Sepharose beads (100 μl). Biotinylated proteins on the beads were washed three times each with Wash buffer-1 (0.2% SDS in water, protease inhibitors), Wash buffer-2 (0.1% deoxycholate, 1% Triton X-100, 500 mM NaCl, 1 mM EDTA, 50 mM HEPES pH 7.5, protease inhibitors), Wash buffer-3 (50 mM LiCl, 0.5% NP40, 0.5% deoxycholate, 1 mM EDTA, 10 mM Tris pH 8.1, protease inhibitors), Wash buffer-

4 (50 mM Tris pH 7.4, 50 mM NaCl, protease inhibitors), and eluted from the beads with elution buffer (2% SDS, 20% glycerol, 62.5 mM Tris–HCl, pH 6.8, 0.01% bromophenol blue, 2 mM biotin) and heating to 95°C for 5 min. Eluted proteins were then probed by immunoblot for BER/SSBR proteins and replication marker proteins.

Graphics

The Graphical Abstract was created in BioRender. Sobol, R. (2025) https://BioRender.com/s2×0qaw. The graphics for Figs 2A and B and 7G were also created in BioRender, as described in the figure legends.

Data analysis

Data are shown as the mean ± standard deviation from 2–3 independent experiments. The Student's *t*-test was used for comparisons between the two groups. Two-way ANOVA was used for multiple comparisons. The significance between the control and experimental groups is indicated by *P*-values. *P*-values are indicated by asterisks with $^{*}P < .05$, $^{**}P < .01$, $^{***}P < .001$, $^{****}P < .0001$. GraphPad PRISM v10.5.0 was used for statistical analysis. Synergy calculations were made using the Bliss independence model [97], essentially as we have described previously [75]. Briefly, an Excess Over Bliss value above 0 indicates synergy, while a score of 0 indicates independent additivity and a score less than zero indicates antagonism between the two drugs, as described in [97].

Results

PAR is synthesized in a PARP1, PARP2, and replication-dependent manner

Both PARP1 and PARP2 contribute to DNA damage-induced PAR synthesis [13, 98]. In GSCs, we have recently shown that both DNA damage-induced and replication-dependent PARylation are enhanced when supplemented with the NAD^+ precursor NRH [30, 31]. PARG inhibitor (PARGi)-induced accumulation of PAR in GSCs is primarily dependent on PARP1 [31], while in several other cancer cells, PARP2 was found to have a minor but important role in DNA damage-induced and replication-dependent PARylation [13, 30, 31]. We have expanded on these studies here to define the involvement of both PARP1 and PARP2 in replication-dependent PARylation. We selected ES-2 cells, an ovarian cancer cell line reported to have a high level of replication stress [99, 100], and the glioma cell line LN428 that contains a mutation in *TP53* and a deletion of the p16(INK4a) (*CDKN2A*) gene [101–104], also giving rise to elevated levels of replication stress [105, 106].

To reveal the level of replication-dependent PAR accumulation [107], PAR levels were evaluated by immunoblot in asynchronously cycling LN428 and ES-2 cells that were exposed for 8 h to NRH (100 μM), the model PARG inhibitor PDD00017273 (10 μM), or NRH + PARGi, with DMSO-exposed cells used as controls. Consistent with our earlier studies [31], PARGi treatment stabilized PAR levels that were further elevated in the presence of the NAD^+-precursor NRH in both LN428 cells (Fig. 1A) and ES-2 cells (Fig. 1B). To define the role of both PARP1 and PARP2 in response to replication stress, we used CRISPR/Cas9 to create PARP1-KO, PARP2-KO, and double PARP1/PARP2-KO in LN428 cells (Fig. 1C). Consistent with our earlier studies on laser-induced DNA damage [13], PAR levels were significantly reduced in the PARP1-KO cells as compared to the levels of PAR in the parental LN428 cells (Fig. 1D). Interestingly, the PAR chain length appears longer in the PARP2-KO cells, which is in line with earlier studies suggesting a role for PARP2 in PAR branching [108], while no PAR was observed in the double knockout LN428/PARP1-KO/PARP2-KO cells (Fig. 1D). As expected from our previous reports [30, 31], combining the PARGi PDD00017273 with the NAD^+ precursor molecule NRH led to an increase in PAR formation, as compared to PARGi alone (Fig. 1A, B, and D). Overall, these studies confirm that both PARP1 and PARP2 are required for PAR synthesis in asynchronously cycling LN428 and ES-2 cells.

To evaluate whether PARP1/PARP2-mediated PARylation is dependent on replication, LN428 cells were synchronized in G1 by serum starvation. Cell synchronization in G1 and release into the S phase was confirmed using flow cytometric-based cell cycle analysis (Supplementary Fig. S1A), which showed that releasing serum-starved cells caused them to slowly enter S phase in a time-dependent manner. Comparing PAR formation in replicating and non-replicating LN428 cells showed that PAR is synthesized in a replication-dependent manner (Fig. 1E and Supplementary Fig. S1B). Replication-dependent PAR formation was also confirmed in ES-2 cells by synchronizing cells with a double thymidine block (Fig. 1F and Supplementary Fig. S1D). PAR immunoblot of both the LN428 cells and the ES-2 cells shows excessive PAR formation within a short time after release into S phase, as compared to non-replicating cells (Fig. 1E and F and Supplementary Fig. S1B).

PARP1-mediated, replication-dependent PARylation recruits BER/SSBR factors XRCC1, POLB, APTX, and LIG3

DNA damage-induced PARP1 activation and the synthesis of PAR facilitate the recruitment of PAR-binding proteins such as XRCC1 that, in turn, recruit additional DNA repair factors via heterodimerization with XRCC1 [8, 10, 13, 14]. To identify proteins recruited to sites of replication-dependent PARP1 activation, we developed both a two-vector and a single-vector PARP1/XRCC1 Split-TurboID proximity labeling system [109], whereby proteins are biotinylated when the PARP1–XRCC1 complex is formed following PARP1 activation (Fig. 2A) and the TurboID protein is re-formed, allowing biotinylation of proximal proteins. Both an LN428 and an ES-2 cell line were created that each expresses Split-TurboID fusions for both PARP1-TurboC and XRCC1-TurboN. In this system, TurboID reconstitution (Turbo-N/Turbo-C) and biotinylation depend on the interaction of PARP1 with XRCC1, and in turn, biotinylated proteins can then be captured using magnetic streptavidin beads (Fig. 2B).

To biotinylate BER/SSBR proteins that are recruited by the PARP1/XRCC1 complex in response to replication, the LN428/PARP1–XRCC1/Split-TurboID cells were synchronized using serum starvation (Fig. 2A and B). Cell synchronization was confirmed by cell cycle analysis (Supplementary Fig. S1C). Replicating and non-replicating cells were then supplemented with biotin (100 μM) for 1 h, followed by streptavidin pull-down and immunoblotting to probe for key BER/SSBR factors (Fig. 2B and C). In line with PAR levels ± replication (Fig. 1E and F and Supplementary Fig. S1B), we observed an increase in biotinylation of both PARP1 and XRCC1

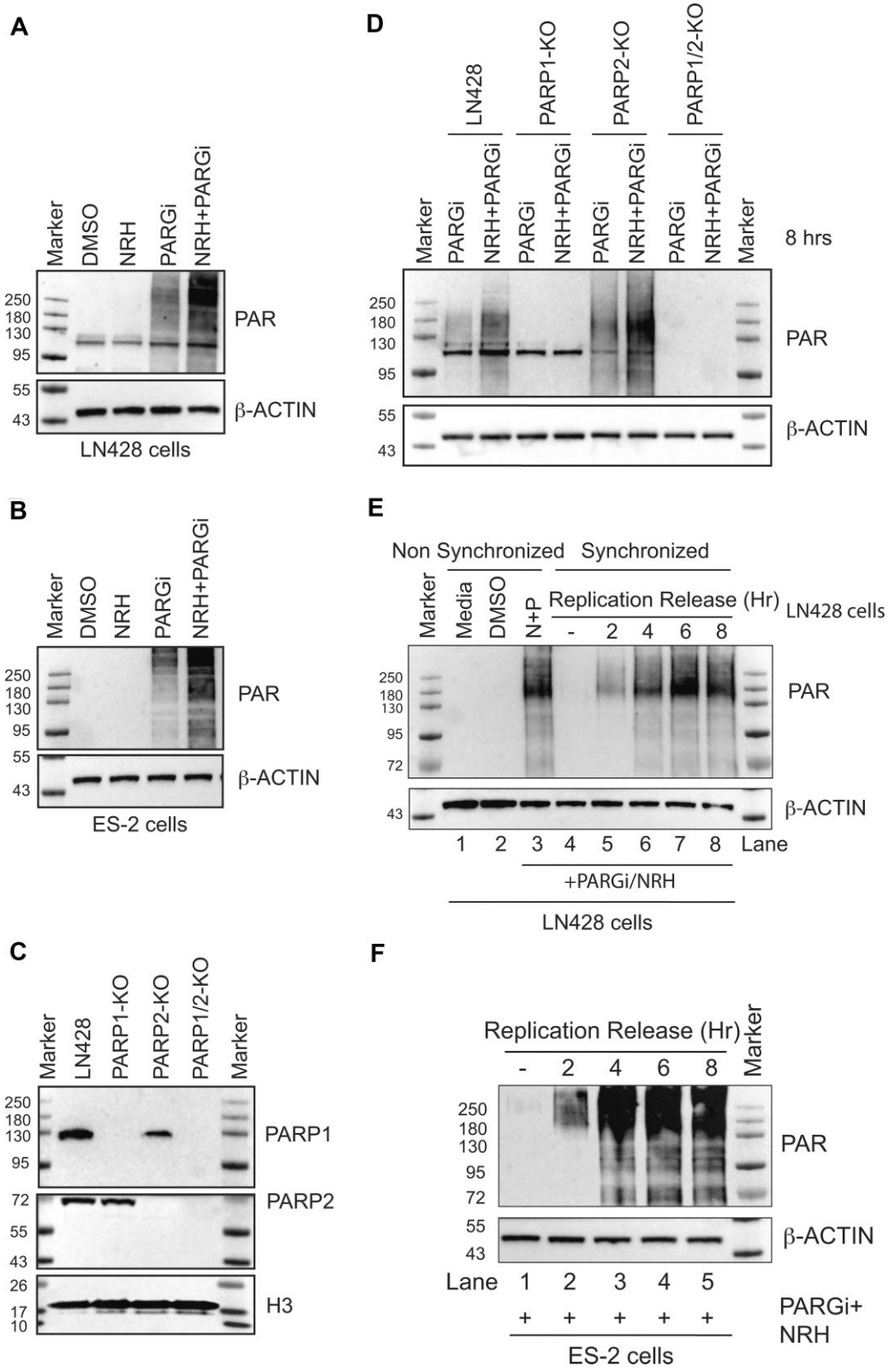

Figure 1. Replication-dependent PARP1/PARP2 activation. (**A**) PAR immunoblot of whole cell lysates prepared from LN428 cells exposed to vehicle (DMSO), NRH (100 μM), PARGi (PDD00017273, 10 μM), or NRH + PARGi for 8 h, with β-ACTIN shown as a loading control. (**B**) PAR immunoblot of whole cell lysates prepared from ES-2 cells exposed to vehicle (DMSO), NRH (100 μM), PARGi (PDD00017273, 10 μM), or NRH + PARGi for 8 h, with β-ACTIN shown as a loading control. (**C**) Immunoblot of PARP1, PARP2, and H3 (loading control) documenting PARP1-KO, PARP2-KO, and PARP1 + PARP2 double-KO via CRISPR/Cas9 in LN428 cells. (**D**) PAR immunoblot of whole cell lysates prepared from LN428, LN428/PARP1-KO, LN428/PARP2-KO, and LN428/PARP1-KO/PARP2-KO cells exposed to PARGi (PDD00017273) or NRH + PARGi for 8 h, with β-ACTIN shown as a loading control. (**E**) PAR immunoblot of whole-cell lysates prepared from LN428 cells (non-synchronized; Lanes 1–3), following serum starvation (synchronized/non-replicating cells; G1 phase, Lane 4), and after release following normal media replenishment (replicating; S-phase, Lanes 5–8). (**F**) PAR immunoblot of whole cell lysates prepared from ES-2 cells following double thymidine block (synchronized/non-replicating cells; G1 phase, Lane 1) and after release following normal media replenishment (replicating; S-phase, Lanes 2–5), with β-ACTIN shown as a loading control.

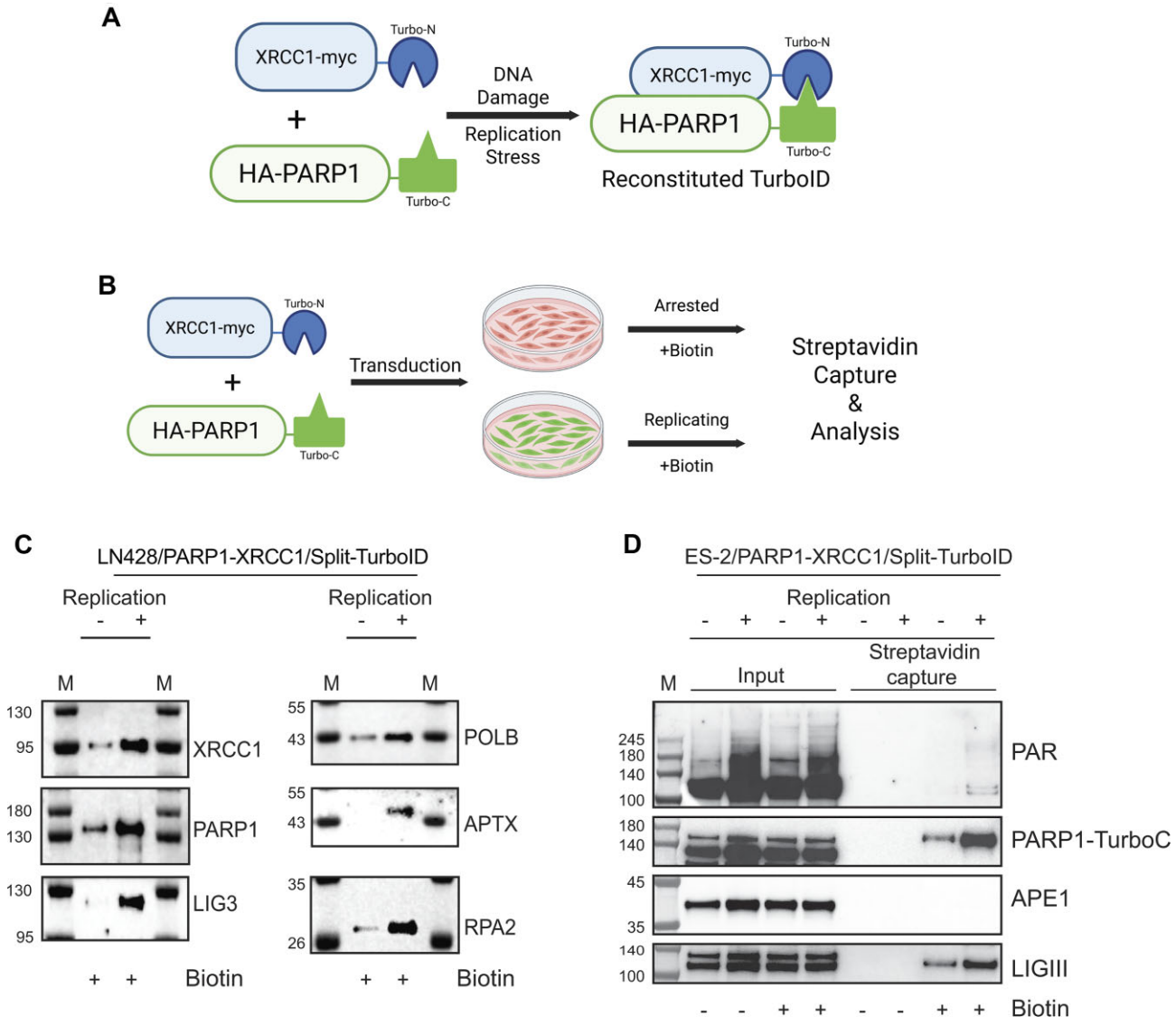

Figure 2. Identification of BER/SSBR factors during replication. (**A**) Graphic depicting the PARP1–XRCC1 Split-TurboID system. The biotinylation protein TurboID was split into an N-terminal domain (Turbo-N) and a C-terminal domain (Turbo-C). The Turbo-N domain was fused in-frame to the C-terminus of XRCC1, while the Turbo-C domain was fused in-frame to the C-terminus of PARP1. Upon the induction of DNA damage or replication stress, the co-localization of XRCC1 and PARP1 causes the reassembly and activation of TurboID and the initiation of proximity biotinylation [96, 109]. Created in BioRender. Sobol, R. (2025) https://BioRender.com/p82xg0b. (**B**) Graphic depicting the experimental outline of proximity labeling (PARP1–XRCC1/Split-TurboID) to capture activated PARP1–XRCC1 complexed proteins during replication. Created in BioRender. Sobol, R. (2025) https://BioRender.com/zoadg6m. (**C**) Streptavidin capture of biotinylated proteins in LN428/PARP1–XRCC1/Split-TurboID cells. Cells were arrested by serum starvation and then released from the block by media change. Arrested (–) and actively replicating (+) cells were exposed to biotin (100 μM, 60 min) for 1 h. Biotinylated proteins were captured with streptavidin-coated beads and probed by immunoblot. (**D**) Streptavidin capture of biotinylated proteins in ES-2/PARP1–XRCC1/Split-TurboID cells. Cells were arrested in G1 for 48 h by CDK4/6 inhibition and then released from the block by media change. All cells were exposed to 10 μM PARGi and 100 μM NRH for 6 h, and biotinylation was then performed with 100 μM biotin for 1 h. Biotinylated proteins were captured with streptavidin-coated beads and probed by immunoblot.

in replicating cells as compared to arrested cells (Fig. 2C). It is noted that there is a low level of PARP1 and XRCC1 biotinylation in resting cells (Fig. 2C and D), suggesting there is evidence for minimal PARP1/XRCC1 complex formation in G1. However, consistent with the elevated levels of PAR upon replication, we find there is elevated replication-dependent activation/formation of the PARP1/XRCC1 complex in S-phase that then facilitates the interaction with the BER/SSBR proteins POLB, APTX, and LIG3 in LN428 cells (Fig. 2C) and recruitment of LIG3 in ES-2 cells (Fig. 2D). This is consistent with our earlier studies on the capture and identification of PAR-complexed proteins in response to alkylation damage [10]. However, unique to this study, we also find the replication marker RPA2 (Fig. 2C). However, consistent with a role for the BER factor APE1 acting upstream of PARP1 [20], we did not observe recruitment of APE1 upon PARP1 activation and formation of the PARP1/XRCC1 complex (Fig. 2D). Similarly, using PARP1-BioID analysis in arrested and replicating cells, we found enhanced biotinylation of XRCC1, PCNA, and ORC2 in replicating cells due to proximity to PARP1 [31]. In all, we suggest this confirms that BER and SSBR proteins are recruited to activated PARP1 during replication, likely in re-

sponse to replication stress-induced PARP1 activation, which we term replication-associated BER/SSBR.

XRCC1, POLB, APTX, and LIG3 suppress replication-dependent PARylation

In GSCs, loss of the BER/SSBR factor XRCC1 or inhibition of the BER enzyme FEN-1 significantly enhanced the level of replication-dependent PAR [31], consistent with the accumulation of BER intermediates [110, 111], unprocessed Okazaki fragments [67], and/or the accumulation of single-stranded DNA gaps [46], each shown to enhance PARP1 activation. Further, loss of XRCC1 or POLB enhances binding of PARP1 and PARP2 to sites of DNA damage, promoting continued PARylation [13]. We therefore hypothesized that the loss of these BER/SSBR factors would impact the level of PARylation in replicating cells.

To test this, XRCC1, POLB, APTX, and LIG3 were knocked out in LN428 cells, and PAR levels in LN428/XRCC1-KO (Fig. 3A), LN428/POLB-KO (Fig. 3B), LN428/APTX-KO (Fig. 3C), and LN428/LIG3-KO (Fig. 3D) cells were analyzed upon NRH, PARGi, or NRH + PARGi exposure by immunoblot, as compared to a DMSO control and to the parental LN428 cells. Consistent with studies from us and others, endogenous PAR levels are drastically enhanced upon PARGi or NRH + PARGi treatment in the BER/SSBR-depleted cells, as compared to the parental LN428 cells. To validate this finding and to demonstrate the cell line independence of PARylation suppression by XRCC1, POLB, APTX, and LIG3, these BER/SSBR factors were also knocked out in the ES-2 cell line. Similarly, ES-2/XRCC1-KO (Fig. 3E), ES-2/POLB-KO (Fig. 3F), ES-2/APTX-KO (Fig. 3G), and ES-2/LIG3-KO (Fig. 3H) cells exposed to PARGi or NRH + PARGi showed enhanced PARylation compared with the parental ES-2 cells. Conversely, no increase in PAR is observed in APE1-KO cells exposed to NRH + PARGi (Supplementary Fig. S2). Overall, these studies validate that XRCC1, POLB, APTX, and LIG3 each contribute to the suppression of endogenous PARylation in response to replication stress, revealed by PARG inhibition.

Depletion of XRCC1, POLB, APTX, and LIG3 overcomes PARP inhibitor resistance

The elevated level of PARP1/PARP2 activation in the LN428 and ES-2 cells depleted of the BER/SSBR scaffold protein XRCC1, and of the BER/SSBR factors POLB, APTX, and LIG3, suggests the accumulation of PARP1/PARP2 substrates such as single-stranded DNA gaps [46] that may arise from Okazaki fragment processing defects [67]. As single-stranded DNA gaps are suggested to be a major indicator of PARP-inhibitor responsiveness [44, 112], we next evaluated if loss of these BER factors increased cellular sensitivity to a panel of PARP1/PARP2 inhibitors.

The cell-killing efficacy of PARP inhibitors was found to be associated with the ability of the inhibitor to trap the enzymes (PARP1/PARP2) at the site of DNA damage [113]. It was then determined that homologous recombination enzymes, as well as numerous additional DNA repair enzymes, are involved in the repair of the trapped PARP1/PARP2-DNA complex, including POLB and FEN1, among other DDR pathway proteins [113]. We therefore tested a panel of PARP1/PARP2 inhibitors (Supplementary Fig. S3A), with varying degrees of efficacy and specificity. Based on the mechanism of action and repair of these PARP-trappers [113, 114], we evaluated the response of each compound following exposure to the LN428 and ES-2 parental cells and the corresponding XRCC1-KO cells (Fig. 4A–D and Supplementary Fig. S3B–D). Of these, BMN-673 showed the strongest effect in the XRCC1-KO cells (Fig. 4B and D), considered to be the strongest or most effective of the PARP-trappers [114].

To expand our analysis, we selected PARP inhibitor-sensitive (BRCA2 mutated) PEO1 cells and PARP inhibitor-resistant (BRCA2 proficient) C4-2 cells. We treated both with the PARP inhibitor BMN-673 for 120 h (5 days) and confirmed that the PEO1 cells are sensitive to PARP inhibitors while the BRCA2-proficient C4-2 cells are resistant [85], as expected (Fig. 4F). To determine if loss of BER can overcome the resistance of C4-2 cells to PARP inhibition, XRCC1, POLB, APTX, and LIG3 were each knocked out via Cas9 gene editing. As shown, C4-2/XRCC1-KO (Fig. 4E), C4-2/POLB-KO (Fig. 4G), C4-2/APTX-KO (Fig. 4I), and C4-2/LIG3-KO (Fig. 4K) cells were exposed to the PARPi for 120 h (5 days). Like the enhanced sensitivity seen in the LN428/XRCC1-KO and ES-2/XRCC1-KO cells (Fig. 4B and D), loss of XRCC1, POLB, APTX, or LIG3 each leads to an increase in PARPi sensitivity (Fig. 4F, H, J, and L), albeit to varying degrees.

Depletion of XRCC1, POLB, APTX, or LIG3 overcomes PARGi resistance

In our previous studies, head and neck cancer cells, as well as GSCs, were resistant to PARGi-induced cell killing [31, 75]. However, each showed enhanced PARGi-induced PAR levels and increased PARGi-induced apoptotic cell death when POLB or XRCC1 was depleted. We therefore hypothesized that PARG inhibitor-resistant cell lines utilize the BER/SSBR proteins XRCC1, POLB, APTX, and LIG3 to suppress PARP1/PARP2-mediated PAR in response to replication stress, and therefore, depletion of BER/SSBR proteins should overcome PARGi resistance in the glioma and ovarian cell lines under study herein. To test this hypothesis, the PARGi-resistant cell lines LN428 and ES-2, and their XRCC1, POLB, APTX, and LIG3 knockout derivatives, were compared for the response to PARGi treatment. Consistent with our earlier studies, the LN428/XRCC1-KO (Fig. 5A), LN428/POLB-KO (Fig. 5B), LN428/APTX-KO (Fig. 5C), and LN428/LIG3-KO (Fig. 5D) cells showed enhanced response to increasing doses of PARGi. Next, caspase-3/7 activity, after 48 h, was evaluated in LN428 cells and the corresponding LN428/KO cells upon PARGi (10 μM) treatment. In line with the cell-killing analyses (Fig. 5A–D), cells with a loss of these BER/SSBR factors all showed an increase in PARGi-induced apoptosis (Fig. 5E–H).

To validate that the loss of XRCC1, POLB, APTX, and LIG3 can overcome PARGi resistance in a second cancer cell line, ES-2, ES-2/XRCC1-KO, ES-2/POLB-KO, ES-2/APTX-KO, and ES-2/LIG3-KO cells were exposed to increasing doses of PARGi. Compared to the non-responsive ES-2 cells, the ES-2/XRCC1-KO (Fig. 5I), ES-2/POLB-KO (Fig. 5J), ES-2/APTX-KO (Fig. 5K), and ES-2/LIG3-KO (Fig. 5L) cell lines were significantly more sensitive to PARGi treatment. In addition, these ES-2/KO cell lines showed significantly stronger activation of caspase-3/7 upon PARGi exposure (Fig. 5M–P),

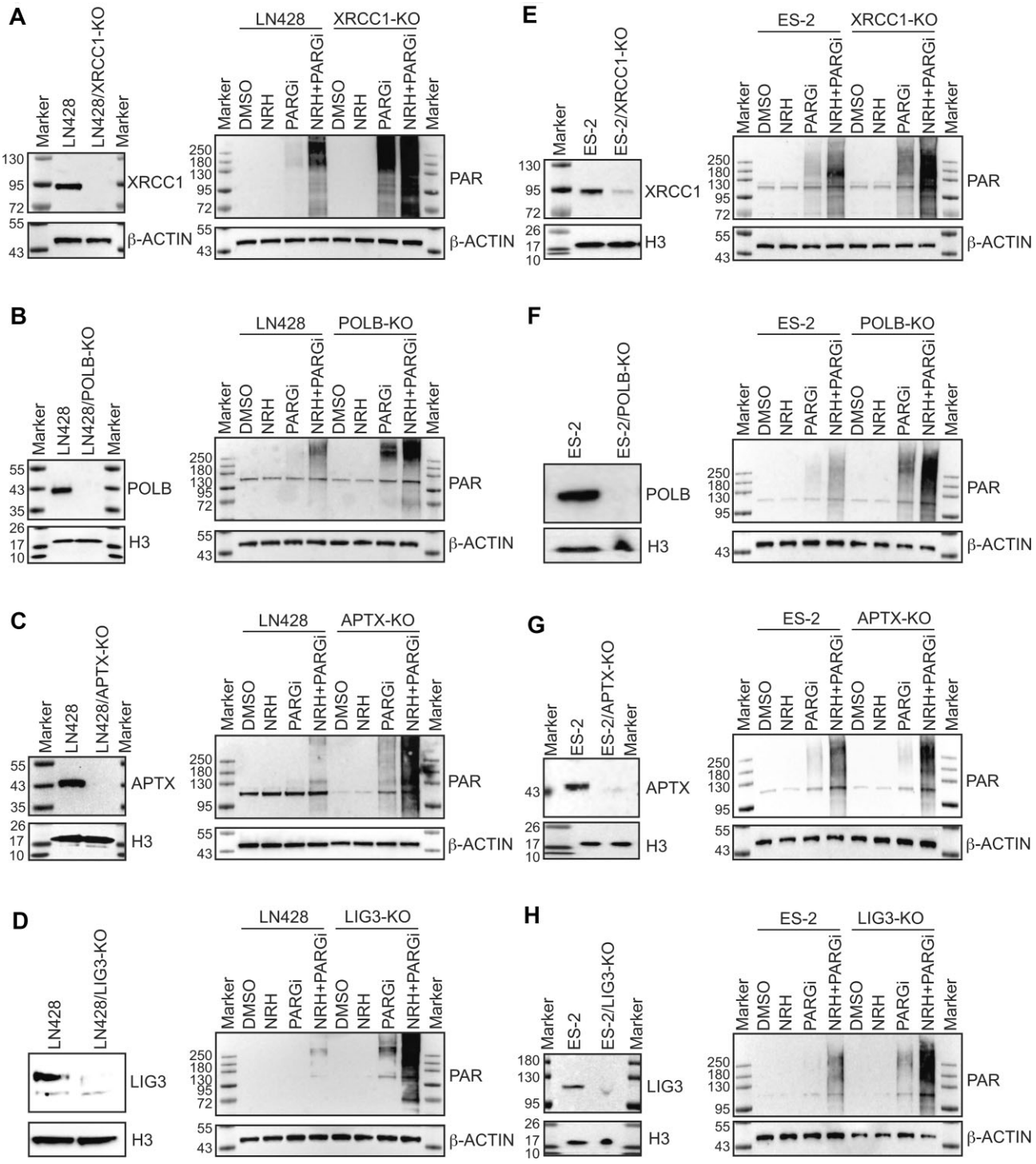

Figure 3. BER/SSBR factors XRCC1, POLB, APTX, and LIG3 regulate PARylation in response to replication stress. Immunoblot of (**A**) LN428 and LN428/XRCC1-KO, (**B**) LN428 and LN428/POLB-KO, (**C**) LN428 and LN428/APTX-KO, (**D**) LN428 and LN428/LIG3-KO, (**E**) ES-2 and ES-2/XRCC1-KO, (**F**) ES-2 and ES-2/POLB-KO, (**G**) ES-2 and ES-2/APTX-KO, and (**H**) ES-2 and ES-2/LIG3-KO whole cell lysates. Blots on the left show the respective knockout of XRCC1, POLB, APTX, or LIG3. The blots on the right show the comparative analysis of replication-dependent PAR formation following 8 h exposure of cells to vehicle (DMSO), NRH (100 μM), PARGi (PDD00017273, 10 μM), or NRH + PARGi. β-ACTIN or H3 was used as a loading control.

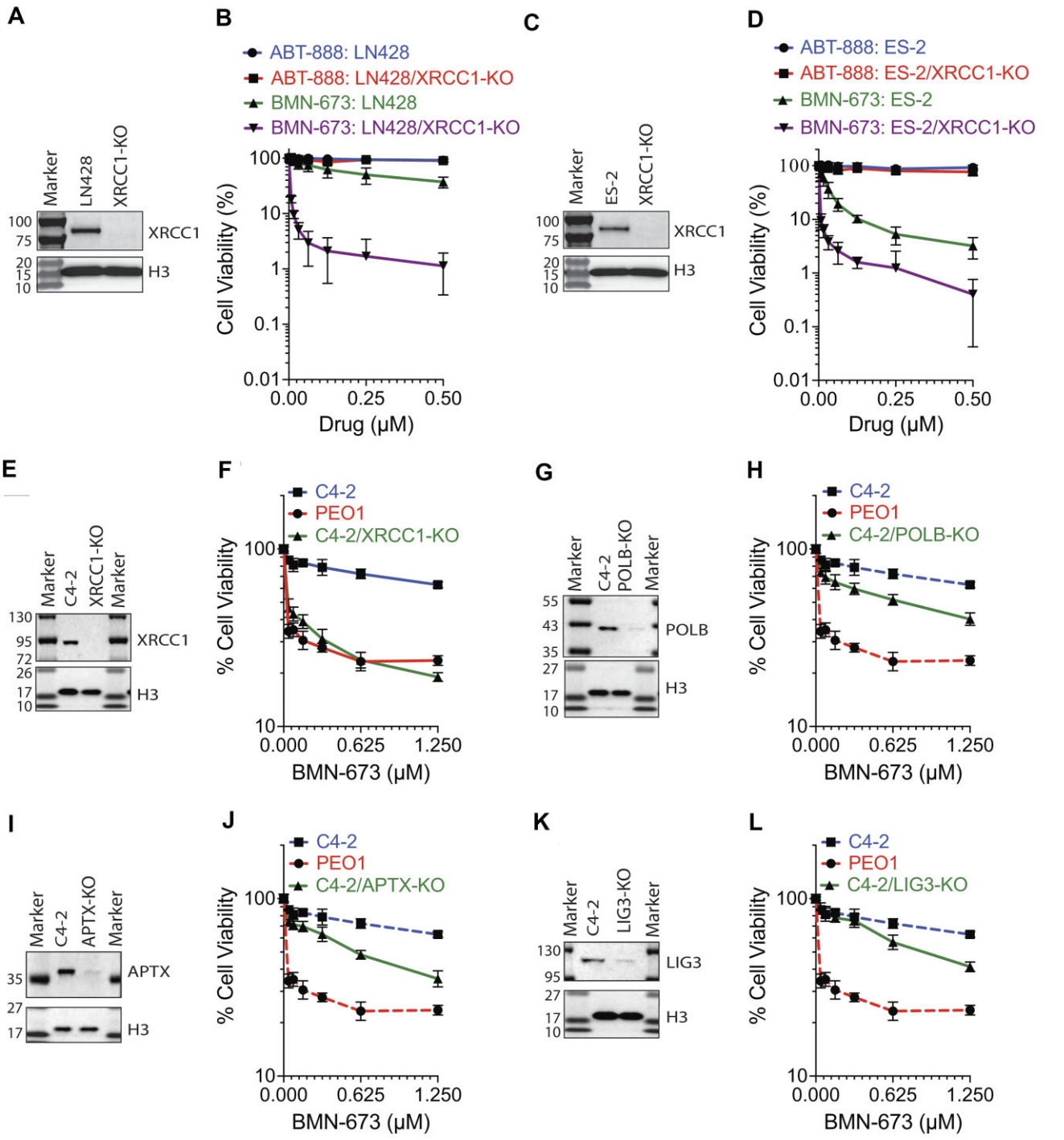

Figure 4. BER/SSBR depletion overcomes PARPi resistance in glioblastoma and ovarian cancer cells. (**A**) Immunoblot for XRCC1 in LN428 and LN428/XRCC1-KO cells, with H3 used as a loading control. (**B**) Viable LN428 and LN428/XRCC1-KO cells (%) exposed to either ABT-888 or BMN-673. (**C**) Immunoblot for XRCC1 in ES-2 and ES-2/XRCC1-KO cells, with H3 used as a loading control. (**D**) Viable ES-2 and ES-2/XRCC1-KO cells (%) exposed to either ABT-888 or BMN-673. (**E**) Immunoblot for XRCC1 in PARP inhibitor-resistant C4-2 and C4-2/XRCC1-KO cells, with H3 used as a loading control. (**F**) Viable cells (%) in response to BMN-673 exposure: PEO1, C4-2, and C4-2/XRCC1-KO cells. (**G**) Immunoblot for POLB in C4-2 and C4-2/POLB-KO cells, with H3 used as a loading control. (**H**) Viable cells (%) in response to BMN-673 exposure: PEO1, C4-2, and C4-2/POLB-KO cells. (**I**) Immunoblot for APTX in C4-2 and C4-2/APTX-KO cells, with H3 used as a loading control. (**J**) Viable cells (%) in response to BMN-673 exposure: PEO1, C4-2, and C4-2/APTX-KO cells. (**K**) Immunoblot for LIG3 in C4-2 and C4-2/LIG-KO cells, with H3 used as a loading control. (**L**) Viable cells (%) in response to BMN-673 exposure: PEO1, C4-2, and C4-2/LIG3-KO cells. For panels (H), (J), and (L), the dotted lines were taken from panel (F) to simplify comparison between the knockouts and C4-2 and PEO1 cells. For panels (B), (D), (F), (H), (J), and (L), viability was assayed after 120 h of exposure to the indicated compounds.

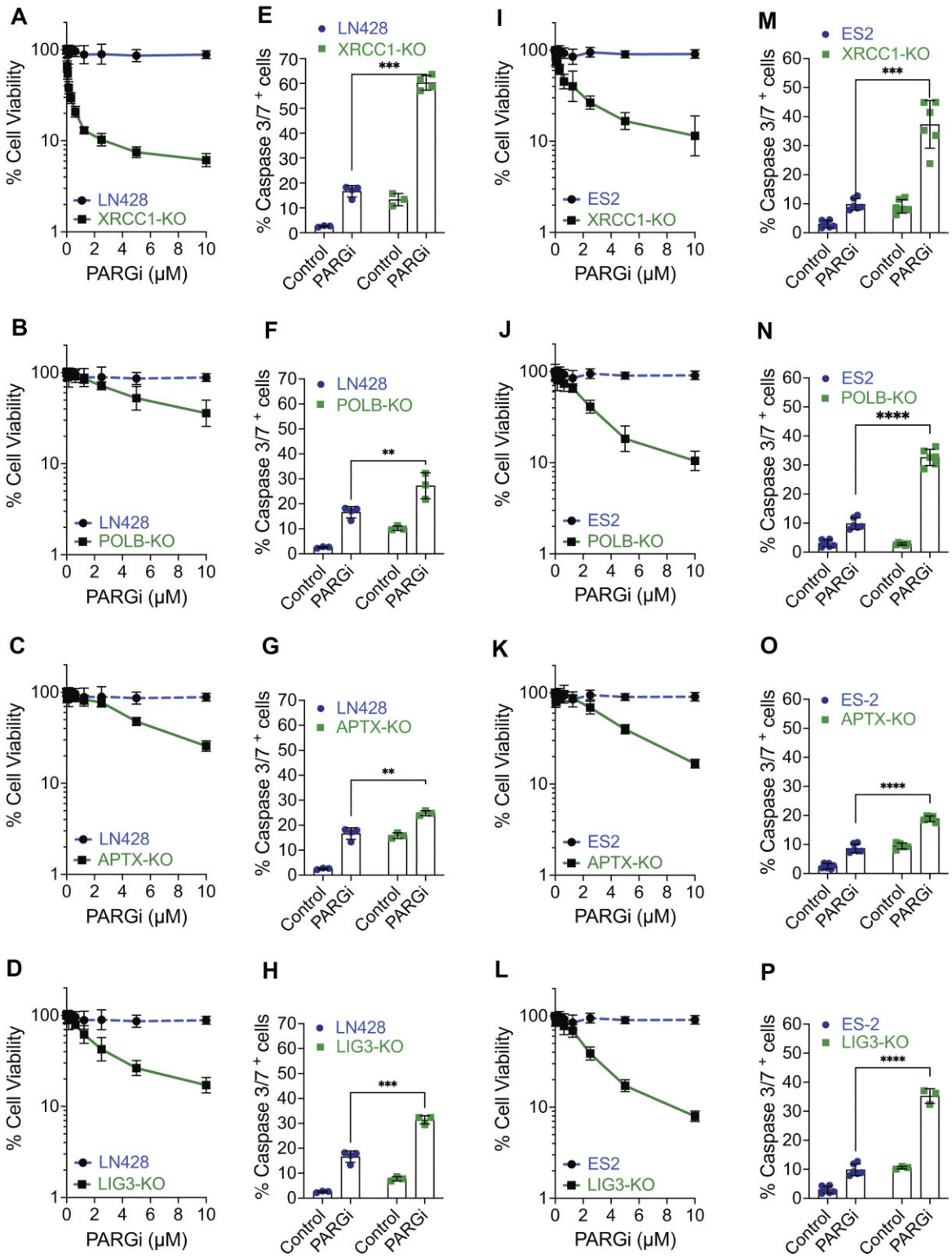

Figure 5. BER/SSBR depletion overcomes PARGi resistance in glioblastoma and ovarian cancer cells. Viable cells (%) in response to PARGi (PDD00017273) in (**A**) LN428 and LN428/XRCC1-KO cells, (**B**) LN428 and LN428/POLB-KO cells, (**C**) LN428 and LN428/APTX-KO cells, or (**D**) LN428 and LN428/LIG3-KO cells. Cells (%) showing caspase-3/7^{+} activity in response to PARGi (PDD00017273) in (**E**) LN428 and LN428/XRCC1-KO cells, (**F**) LN428 and LN428/POLB-KO cells, (**G**) LN428 and LN428/APTX-KO cells, or (**H**) LN428 and LN428/LIG3-KO cells. Viable cells (%) in response to PARGi (PDD00017273) in (**I**) ES-2 and ES-2/XRCC1-KO cells, (**J**) ES-2 and ES-2/POLB-KO cells, (**K**) ES-2 and ES-2/APTX-KO cells, or (**L**) ES-2 and ES-2/LIG3-KO cells. Cells (%) showing caspase-3/7^{+} activity in response to PARGi (PDD00017273) in (**M**) ES-2 and ES-2/XRCC1-KO cells, (**N**) ES-2 and ES-2/POLB-KO cells, (**O**) ES-2 and ES-2/APTX-KO cells, or (**P**) ES-2 and ES-2/LIG3-KO cells. For the viability assays, viability was assayed after 120 h of exposure to the indicated compound, and for the caspase activation assays, the activation of caspase-3/7^{+} was assayed 48 h after drug exposure. For panels (B), (C), and (D), the dotted line was taken from panel (A) to simplify the comparison between LN428 and the corresponding knockout cells. For panels (J), (K), and (L), the dotted line was taken from panel (I) to simplify the comparison between ES-2 and the corresponding knockout cells. Where indicated, $P <$ * .05, $P <$ ** .01, $P <$ *** .001, $P <$ **** .0001; two-way ANOVA.

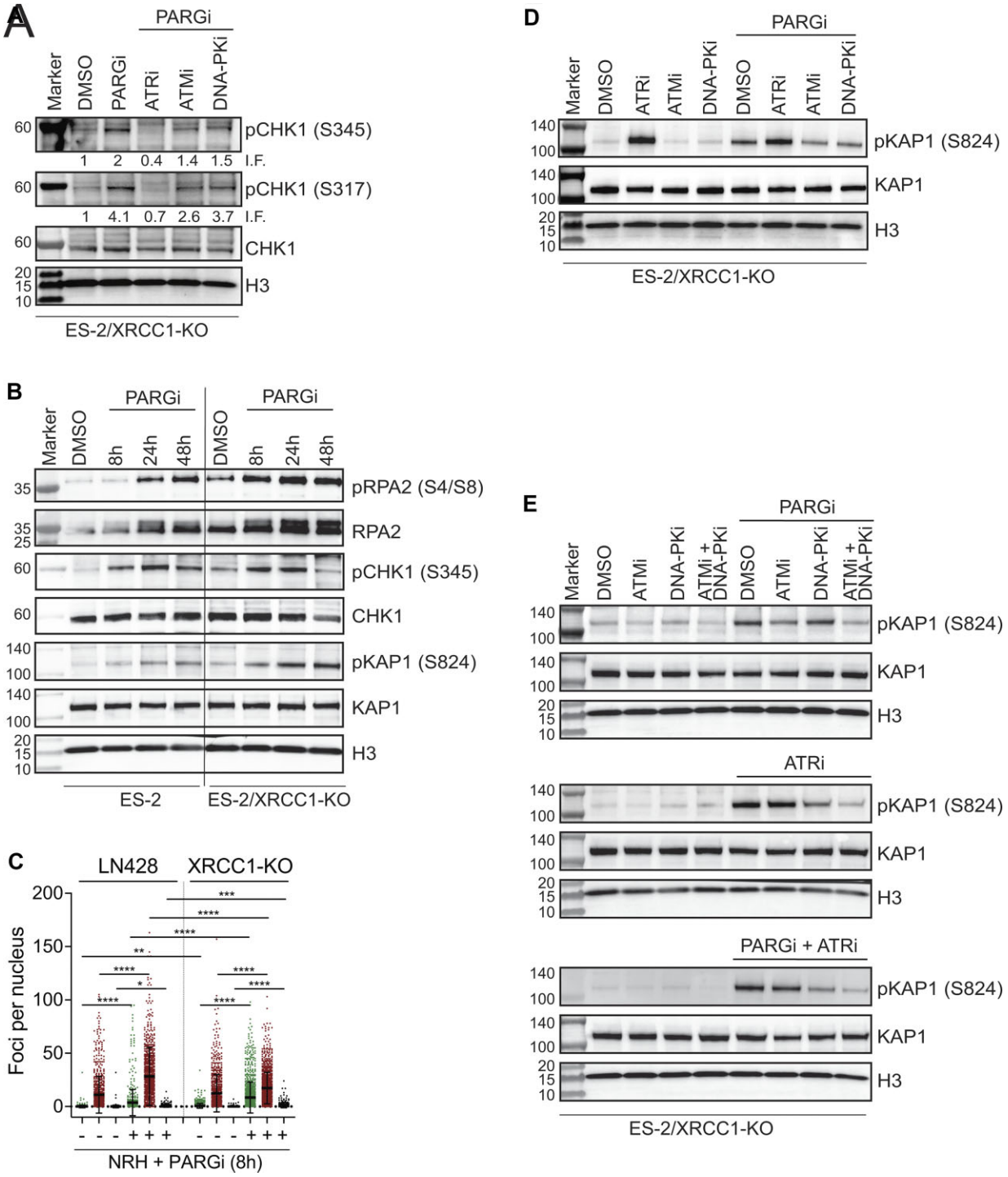

Figure 6. Targeting the S-phase checkpoint overcomes PARGi resistance in glioblastoma and ovarian cancer cells. (**A**) Immunoblot of ES-2/XRCC1-KO whole cell extracts for pCHK1(S345), pCHK1(S317), and CHK1, with H3 used as a loading control. The induction factor (I.F.) for CHK1 phosphorylation was determined by densitometry analysis and is listed under each lane. Cells were exposed to vehicle control (DMSO), ATRi (AZD6738, 10 μM), ATMi (KU-55933, 10 μM), DNA-PKi (KU-57788, 10 μM), and/or PARGi (PDD00017273, 10 μM) as indicated, for 24 h. (**B**) Immunoblot of ES-2 and ES-2/XRCC1-KO whole cell extracts for pRPA2 (S4/S8), RPA2, pCHK1 (S345), CHK1, pKAP1 (S824), and KAP1, with H3 used as a loading control. Cells were exposed to PARGi (PDD00017273, 5 μM) for the indicated time points, with DMSO as the vehicle control. (**C**) Quantification of PAR (green), pRPA(S4/S8) (red), and PAR/pRPA(S4/S8) co-localized (black) foci. Where indicated, $P <$ * .05, $P <$ ** .01, $P <$ ***.001, $P <$ ****.0001; Student's *t*-test (representative images in Supplementary Fig. S4C). (**D**) Immunoblot of ES-2/XRCC1-KO whole cell extracts for pKAP1 (S824) and KAP1, with H3 used as a loading control. Cells were exposed to vehicle control (DMSO), ATRi (AZD6738, 10 μM), ATMi (KU-55933, 10 μM), DNA-PKi (KU-57788, 10 μM), and/or PARGi (PDD00017273, 10 μM) as indicated for 24 h. (**E**) Immunoblot of ES-2/XRCC1-KO whole cell extracts for pKAP1 (S824) and KAP1, with H3 used as a loading control. Top: Cells were exposed to vehicle control (DMSO), ATMi (KU-55933, 10 μM), DNA-PKi (KU-57788, 10 μM), or ATMi + DNA-PKi, with or without PARGi (PDD00017273, 10 μM) as indicated, for 24 h. Middle: Cells were exposed to vehicle control (DMSO), ATMi (KU-55933, 10 μM), DNA-PKi (KU-57788, 10 μM), or ATMi + DNA-PKi, with or without ATRi (AZD6738, 10 μM) as indicated, for 24 h. Botttom: Cells were exposed to vehicle control (DMSO), ATMi (KU-55933, 10 μM), DNA-PKi (KU-57788, 10 μM), or ATMi + DNA-PKi, with or without ATRi (AZD6738, 10 μM) + PARGi (PDD00017273, 10 μM) as indicated, for 24 h.

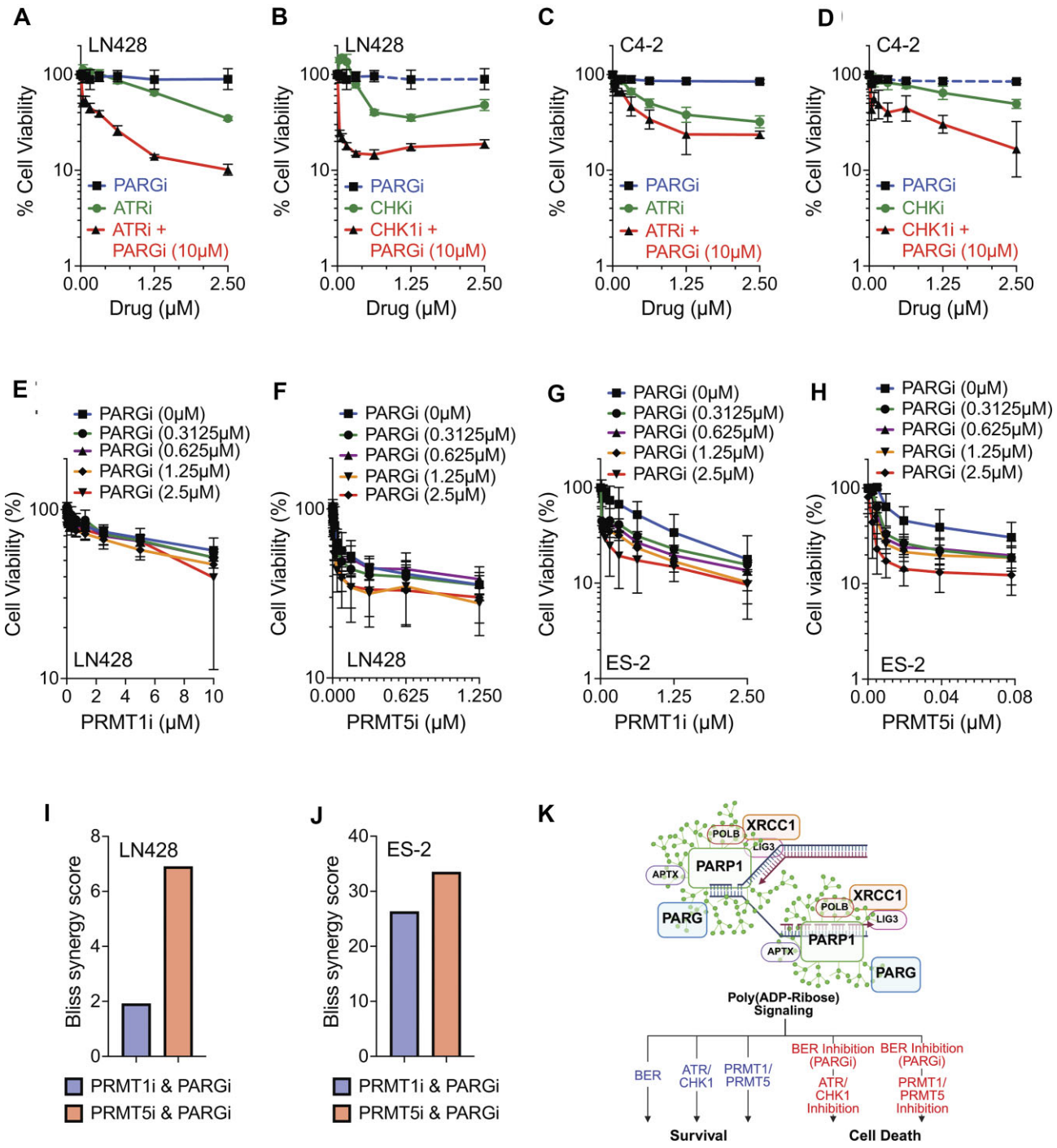

Figure 7. PARGi response enhanced by co-inhibition with CHK1, ATR, and PRMT1i/PRMT5i. (**A**) Viable LN428 cells (%) in response to ATRi (AZD6738), PARGi (PDD00017273), and ATRi + PARGi (10 μM) treatment. (**B**) Viable LN428 cells (%) in response to CHK1i (MK8776), PARGi (PDD00017273), and CHK1i + PARGi (10 μM) treatment. The dotted line was taken from panel (A) for comparison. (**C**) Viable C4-2 cells (%) in response to ATRi (AZD6738), PARGi (PDD00017273), and ATRi + PARGi (10 μM) treatment. (**D**) Viable C4-2 cells (%) in response to CHK1i (MK8776), PARGi (PDD00017273), and CHK1i + PARGi (10 μM) treatment. The dotted line was taken from panel (C) for comparison. For panels (A–D), viable cells were assayed after 120 h of exposure to the indicated compounds. (**E**) Viable LN428 cells (%) in response to PARGi (PDD00017273) and PRMT1i (GSK336871) exposure at the indicated concentrations. (**F**) Viable LN428 cells (%) in response to PARGi (PDD00017273) and PRMT5i (PRT543) exposure at the indicated concentrations. The dotted line was taken from panel (E) for comparison. (**G**) Viable ES-2 cells (%) in response to PARGi (PDD00017273) and PRMT1i (GSK336871) exposure at the indicated concentrations. (**H**) Viable ES-2 cells (%) in response to PARGi (PDD00017273) and PRMT5i (PRT543) exposure at the indicated concentrations. The dotted line was taken from panel (G) for comparison. (**I**) Bliss synergy score for LN428 cells exposed to PARGi and PRMT1i, or PARGi and PRMT5i. (**J**) Bliss synergy score for ES-2 cells exposed to PARGi and PRMT1i, or PARGi and PRMT5i. (**K**) Model for the role of BER/SSBR in suppressing replication stress. Canonical and replication-associated BER/SSBR proteins process replication-stalling DNA lesions. Upon inhibition of BER by PARGi, the inter-S-phase checkpoint is activated via ATR/CHK1. Simultaneous inhibition of PARG and ATR/CHK1 causes cell death, and PRMT1/PRMT5 inhibition-induced cell death is synergistic with PARG inhibition [created in BioRender. Sobol, R. (2025) https://BioRender.com/xke5uat].

like what was observed in the LN428 and LN428/KO cells (Fig. 5E–H).

BER/SSBR factor depletion activates the S-phase checkpoint and enhances PARGi-induced and ATRi-induced replication catastrophe

PARG inhibitor sensitivity correlates with the activation of the S-phase checkpoint [46, 73]. In that regard, we previously found that in head & neck cancer cells, POLB plays a crucial role in modulating the cellular response to PARG inhibition, highlighting POLB-dependent phosphorylation of KAP1, RPA2, and CHK1 [75]. We therefore hypothesized that depletion of the BER/SSBR factors XRCC1, POLB, APTX, and LIG3 would further increase replication stress to activate ATR and the S-phase checkpoint. In line with this hypothesis, PARGi treatment showed ATR-dependent phosphorylation of CHK1, on S345 (Fig. 6A and Supplementary Fig. S4A), as well as on S317 (Fig. 6A), in an XRCC1-regulated manner in ES-2 cells. Further, NRH + PARGi treatment of LN428 cells induced ATR-dependent phosphorylation of CHK1 (Supplementary Fig. S4B). In all cases, activation of pCHK1, as measured by phosphorylation on residue S345, also revealed a minor dependence on ATM & DNA-PK (Fig. 6A and Supplementary Fig. S4A and B).

Given the enhanced PARGi-induced cell death (Fig. 5I), apoptosis (Fig. 5M), and CHK1 activation in the absence of XRCC1 (Fig. 6A), we compared the PARGi-induced replication checkpoint activation in ES-2 versus ES-2/XRCC1-KO cells (Fig. 6B). Consistent with the likely increase in single-stranded DNA gaps [46] and a possible defect in Okazaki fragment processing [67] in the absence of XRCC1, there is an elevated level of phosphorylated RPA2 (S4/S8) in the absence of XRCC1 that is further elevated upon PARGi treatment, as compared to the parental ES-2 cells (Fig. 6B). We also found significant co-localization of PAR and pRPA(S4/6) foci in response to PARGi + NRH treatment that is also XRCC1-dependent (Fig. 6C and Supplementary Fig. S4C).

Further, in addition to the observed increase in phosphorylated CHK1, we found that the most prominent BER/SSBR-dependent, PARGi-induced, checkpoint signal is the phosphorylation of KAP1 on S824 (Fig. 6B). Given that KAP1 is reported to be phosphorylated in an ATM-dependent manner, we evaluated the impact of PARGi-induced and ATRi-induced phosphorylation of KAP1 on S824, alone and following inhibition of the DDR kinases ATM and DNA-PK in the ES-2/XRCC1-KO cells (Fig. 6D and E). Interestingly, ATRi alone, PARGi alone, or ATRi + PARGi gave rise to a strong level of KAP1 phosphorylation with suppression of the signal when combined with ATMi, DNA-PKi, or both (Fig. 6D and E), suggestive of BER/SSBR regulation of PARGi-induced and ATRi-induced replication catastrophe [76, 115].

Since both PARG and ATR inhibition lead to elevated KAP1 phosphorylation, suggestive of replication catastrophe, we anticipated that a combination of ATR and PARG inhibition would lead to an enhanced cell-killing effect. As shown, in both LN428 and C4-2 cells, there was a minor cell-killing effect upon exposure to ATRi (AZD6738), CHK1i (MK8776), or PARGi (PDD00017273) as a single agent (Fig. 7A–D). However, when the CHK1i or the ATRi was combined with the PARGi, we observed a significantly enhanced response (Fig. 7A–D, red lines).

Enhanced PARG inhibitor cell sensitivity upon PRMT1/PRMT5 inhibition

Protein arginine methyltransferases (PRMTs) [79] modify arginine residues with a methyl group via asymmetric (PRMT1) and symmetric (PRMT5) dimethyl substitutions [79]. Primary targets of PRMTs include ATR, 53BP1, and BRCA1 [79], and they are suggested to impact the replication stress response [82]. Further, it has been proposed that the major impact of PRMT1 or PRMT5 inhibition is to suppress DNA repair gene expression [116–118], likely by impacting splicing [119]. Given the enhanced cell killing response observed when combining PARG inhibitors and ATR inhibitors (Fig. 7A and C), and the proposed impact on ATR and the replication stress response by PRMT1 and PRMT5 inhibitors [80, 82, 117, 119], we evaluated the cellular response (LN428 cells and ES-2 cells) to PRMT1 and PRMT5 inhibitors alone, and when combined with sub-lethal doses of the PARG inhibitor PDD00017273 (10 μM). [As shown in Fig. 5A and I, there is <5% cell killing when LN428 or ES-2 cells are treated with PDD00017273 at 10 μM]. Both the LN428 cells (Fig. 7E and F) and the ES-2 cells (Fig. 7G and H) showed a synergistic response when PRMT1 or PRMT5 inhibitors were combined with PARG inhibitors (Fig. 7I and J), with the strongest synergy observed in the ES-2 cells (Fig. 7J).

Overall, these studies suggest a model for the BER/SSBR response to PARP1/PARP2 activation in response to replication stress. As shown (Fig. 7K), the level of PAR induction is regulated by XRCC1 and the XRCC1-binding proteins POLB, APTX, and LIG3, which are further regulated by PARG, all to suppress the activation of the ATR/CHK1 S-phase checkpoint. The activation of the ATR/CHK1 checkpoint promotes survival, whereas PAR-induced cell killing is enhanced when ATR or CHK1 is inhibited. This might suggest a PARG/ATR functional relationship or may be related to a role for ATR inhibition in the induction of DNA damage, such as the recent demonstration that ATR inhibition leads to elevated genomic uracil [120], known to induce replication stress [57, 121]. Further, given the regulatory control of ATR by the methylation transferases PRMT1 and PRMT5, this also suggests a synthetic lethal connectivity node between PARG and PRMT1/PRMT5 (Fig. 7K).

Discussion

The vital importance of genome maintenance and the DDR is underscored by the multiple mechanisms that function to repair specific types or classes of damaged DNA [122, 123]. Of these pathways, the signaling enzyme PARP1 [124], and in some cases PARP2 [125], are involved in the regulation or signaling for BER/SSBR [2, 13, 20], MutSα and MMR [16], and DDB2/XPC in NER-mediated UV damage repair [17, 18], as well as TMEJ [19].

Our studies have focused on the activation of PARP1 and PARP2 and the central role these proteins play in the cellular response to DNA base damage to initiate canonical BER/SSBR [2, 13, 20] (see Graphical Abstract). The resulting activation of PARP1/PARP2 leads to the synthesis of PAR at the site of the genomic insult, forming a scaffold for protein complex assembly to respond to the damage [2] via protein-encoded PAR binding domains [15]. Canonical BER/SSBR responds to base damage or SSBs in all phases of the cell cycle, primarily via DNA glycosylase-mediated lesion hydrolysis and/or APE1-

induced or DNA damage-induced strand cleavage followed by PARP1/PARP2 activation, facilitating the recruitment of the end- and gap-processing proteins XRCC1, POLB, APTX, and LIG3. Once repair is complete, the damage signal (PAR) is removed by the PAR-degrading enzymes PARG, TARG1, and ARH3 [2, 20, 26, 27] (see Graphical Abstract). The requirement for these BER/SSBR proteins is demonstrated by loss or inhibition: BER/SSBR protein deficiency or inhibition leads to DNA damage-induced PAR accumulation and a block to glycolysis [9, 10] or initiation of G2/M arrest [31], depending on the damage type and extent.

Here, we expand our analysis to the activation of PARP1 and PARP2 in response to replication stress to initiate what may be called replication-associated BER/SSBR [8, 30, 31]. We find that replication-dependent PARP1/PARP2 activation and recruitment of XRCC1 and select BER/SSBR factors are essential to suppress replication-stress-mediated PAR accumulation, CHK1 activation [56], and S-phase arrest [30, 31] (see Graphical Abstract). The replication-dependent or replication-stress-dependent substrates of PARP1, as well as PARP2, are varied, including BER/SSBR intermediates [110, 111, 126], Okazaki fragments [67], single-stranded DNA gaps [46, 127], nicks from the repair of misincorporated uracil or from abasic site repair [57, 120, 121, 128, 129], stressed replication forks [130], and transcription-replication conflicts and R-loops [58, 131]. In line with these findings, we find that PAR accumulates in a replication-dependent manner that is dependent on the expression of both PARP1 and PARP2 (Fig. 1). A role for PARP1 during replication has long been suggested [132] as PARP1 was identified as part of a multiprotein DNA replication complex [133] that includes DNA polymerase alpha-primase [134]. PARP1 has also been described as a sensor for Okazaki fragment processing [67], interacts with structures mimicking the replication fork [107], and signals to RECQ1 to suppress replication restart [135]. Further, it was recently found that PARP1 interacts with several additional replication factors, including TIMELESS and TIPIN, DNA translocases, ORC2, and TPX2 [31, 130, 131, 136]. Here we show that both PARP1 and PARP2 give rise to replication-dependent PAR synthesis (Fig. 1), similar to the combined role of both isoforms in DNA damage-induced PAR synthesis [13, 137].

In addition, similar to our findings in GSCs [31], the replication-dependent accumulation of PAR in these glioma (LN428) and ovarian (ES-2) cancer cell lines is enhanced upon supplementation with NRH, an NAD^+-precursor that, when added to cells, can promote as much as a 10-fold increase in nuclear NAD^+ levels, enhancing PARP1/PARP2 activation potential [13, 83]. Consistent with our earlier report on GSCs [31], arrested LN428 or ES-2 cells show very little PAR accumulation (Fig. 1). In the absence of PAR, little to no BER/SSBR factor recruitment is expected [8, 13]. Conversely, replication-dependent PAR synthesis should facilitate the recruitment of the PAR-binding protein XRCC1 and the associated BER/SSBR factors that bind to XRCC1, including POLB, APTX, and LIG3 [8, 138].

To address whether activated PARP1 recruits BER proteins during replication in cancer cells, we developed both a two-vector and a single-vector PARP1/XRCC1 Split-TurboID system, expressed in LN428 and ES-2 cells (Fig. 2). The TurboID system has the advantage of identifying interacting protein partners in cells, in a temporal manner, by proximity biotinylation [96, 109]. Our PARP1–XRCC1/Split-TurboID approach has the added advantage of only labeling proximal protein partners with biotin when PARP1 is bound to XRCC1, upon formation of the PARP1–XRCC1 activated complex [28]. Like the recruitment of key BER/SSBR factors in response to laser-induced DNA damage [13], we find that replication, or replication-stress-dependent PARP1 activation promotes the recruitment of the BER/SSBR scaffold protein XRCC1 and the XRCC1 binding proteins POLB, APTX, and LIG3 (Fig. 2), as well as the replication factor RPA2 that may suggest these BER factors are involved in gap repair [46, 127] or Okazaki fragment processing [67, 139, 140, 141]. However, such activation does not recruit the upstream BER protein APE1, consistent with its role prior to PARP1 activation [2, 20]. Interestingly, the basal level of PARP1 and XRCC1 biotinylation we observed (Fig. 2) suggests there is a low level of PARP1/XRCC1 complex formation in the fraction of resting cells isolated. However, this PARP1/XRCC1 complex formation is only marginally suppressed by pretreatment with a PARP inhibitor (not shown). The extent of PARP inhibitor suppression of the overall levels of basal PARP1/XRCC1 biotinylation and whether this is due to overall oxidative damage or a low level of replication-dependent PARP1 activation in the minor fraction of cells not in G1 remains to be determined.

Cells with DNA repair defects, especially defects in HR, have elevated levels of PAR [142, 143]. Similarly, loss of some BER factors increases spontaneous or DNA damage-induced PAR levels [13, 30, 31]. This may be due to increased binding of PARP1 and PARP2 at sites of DNA damage [13] and/or persistence of PARP1/PARP2-activating repair intermediates [110, 111, 126]. This would suggest that loss of some or all of the BER/SSBR proteins that are recruited to the activated PARP1/XRCC1 complex may lead to prolonged PARP activation or hyper-PARylation [138]. We tested this concept here by CRISPR/Cas9-mediated KO of XRCC1, APTX, POLB, or LIG3 in both the LN428 and ES-2 cells, as well as XRCC1-KO and APE1-KO in RPE-1 cells (Fig. 3 and Supplementary Fig. S2). Consistent with a biological role for these BER/SSBR factors in replicating cells and in line with some earlier reports [31, 110], cells with loss of XRCC1, APTX, POLB, or LIG3, but not APE1, show elevated PAR levels when treated with a PARGi that is further enhanced when co-treated with the NAD^+-precursor NRH (Fig. 3 and Supplementary Fig. S2).

The increased PAR level, seen when some BER/SSBR factors are absent, has been suggested to impact PARP-inhibitor response since the expression of XRCC1 was shown to prevent PARP1 trapping [110] at the site of the damage, and its loss will enhance PARP1/PARP2 binding to the lesion site [13, 110]. This would imply that BER/SSBR defective cells may be hypersensitive to PARP-trapping agents [113, 114]. To that end, we tested a panel of PARP inhibitors (Supplementary Fig. S2) in the LN428 and ES-2 cells and the corresponding XRCC1-KO cells (Fig. 4 and Supplementary Fig. S2). In line with a role for BER/SSBR in preventing PARP1 trapping [110], the most effective PARP inhibitor for XRCC1-KO cells (BMN-673) was previously shown to be the most effective of the PARP trappers [114]. We then expanded our analysis of BER/SSBR involvement in the cellular response to PARP inhibition by developing KOs of XRCC1, APTX, POLB, and LIG3 in C4-2 cells, a PARP-inhibitor-resistant (BRCA2 proficient) ovarian cancer cell line, and compared the response to PARP inhibitor-sensitive (BRCA2 mutated) PEO1 cells. Consistent with the increased PAR levels, the KO cells showed varying

degrees of PARPi sensitivity (Fig. 4). Similarly, several earlier PARPi screens have reported a role for some BER/SSBR proteins in causing PARPi resistance, including POLB, XRCC1, and LIG3 [144–148]. Here, we expand this to also include the BER/SSBR factor APTX and show that each of these BER/SSBR factors (XRCC1, APTX, POLB, and LIG3) appears to suppress spontaneous replication-dependent PAR synthesis, and likely suppress PARP-trapping since they show sensitivity to the PARP-trapping agent BMN-673 (Fig. 4). Further, the elevated PAR levels, when a PARGi is combined with NRH, are another example of how NAD^+ enhances PARP1/PARP2 activation [30, 31, 83].

Although the mechanism of PARGi sensitivity has yet to be completely defined, the elevated levels of replication-dependent PAR observed when BER/SSBR is defective (Fig. 4) also suggest a role for BER/SSBR in regulating or attenuating the cellular response to PARG inhibitors since unrestrained replication-dependent PAR can impact the S-phase replication checkpoint [31, 46, 56, 78]. Deletion of the gene for PARG in mice leads to early embryonic lethality and enhanced sensitivity to DNA-damaging agents [149] and, in human cells, is required for S-phase progression [150]. Further, PARG inhibitors have been shown to enhance the cellular response to temozolomide [30, 151] and to induce replication fork collapse [76], with increased response in BRCA2-defective cell lines [152]. Recently, we have suggested that the level of replication-dependent PAR correlates with PARG inhibitor sensitivity, demonstrating that enhanced PARylation, mediated by the NAD-boosting precursor NRH, significantly impacts the PARG inhibitor response [30, 31]. One possible mechanism offered to explain cell sensitivity to PARG inhibitors is the accumulation of reversed forks [54] or of single-strand DNA gaps during replication [46], the latter similar to recent models for PARP-inhibitor sensitivity [44]. Here, we also find that the BER/SSBR factors XRCC1, APTX, POLB, and LIG3 provide varying degrees of resistance to the model PARG inhibitor PDD00017273 (Fig. 5). The mechanistic explanation for the varied response is forthcoming in future studies, but may be related to possible unique roles that each play in response to PARP1/PARP2 activation. For example, the scaffold protein XRCC1 is expected to have the strongest phenotype, as observed, since XRCC1 is essential to both BER and SSBR, and is required for the recruitment of APTX, POLB, and LIG3. Similarly, LIG3 should be involved in all downstream processes requiring a DNA ligase and is likely involved in suppressing single-strand DNA gaps during replication, likely during repair of Okazaki fragments [67, 139, 141]. The precise role for APTX and POLB in suppressing PARP1/PARP2 activation during replication remains to be determined. However, as suggested earlier, suppression of POLB levels shows increased sensitivity to PARG inhibitors in head and neck cancer cells and cells with mutant IDH1 [75, 77], and it is consistent with the apparent synthetic lethality between PARG and the BER/SSBR factor FEN-1 [153], so it may be feasible that POLB plays a backup role in Okazaki fragment processing.

Cell death mediated by unrepaired, replication-induced PAR is thought to be attenuated by ATR/CHK1 activation and initiation of the S-phase checkpoint [31, 46, 56, 75]. Here too, we find that PARGi-induced CHK1 phosphorylation is ATR dependent, with only a minor impact by ATM or DNA-PK inhibition (Fig. 6). Further, the activation of the ATR/CHK1 checkpoint is protective, since inhibitors to either ATR or CHK1 enhanced the cellular response to PARG inhibitors (Fig. 7), as we found in head and neck cancer cells [75]. As mentioned earlier, the enhanced response when PARG inhibitors are combined with ATR inhibitors may also be the result of elevated uracil, a BER substrate. Recently, it was shown that ATR inhibition leads to a rapid increase in genomic DNA contamination with uracil [154]. Given that genomic uracil induces replication stress [121] and can contribute to PAR-induced replication catastrophe [57], the enhanced response to PARGi, when combined with ATRi, may also be a result of elevated repair intermediates and PARP hyperactivation. However, the enhanced sensitivity of the BER/SSBR defective cells to PARG inhibition appears to give rise to ATM/DNA-PK-mediated phosphorylation of the transcriptional regulator KAP1 [155]. While KAP1 is phosphorylated by CHK1 on S473 [156], phosphorylation of KAP1 on S824, as evaluated here, is ATM dependent [157]. This may suggest that BER/SSBR impacts PARG inhibitor-induced accumulation of lesions that trigger replication catastrophe, leading to ATM and DNA-PK activation, and phosphorylation of KAP1 (Fig. 6). This would be consistent with BER/SSBR loss leading to an increase in single-strand DNA gaps during replication that translate to enhanced sensitivity to PARG inhibitors and an increase in DNA double-strand breaks and collapsed replication forks.

Both PARP inhibitors and PARG inhibitors are thought to target cells due to an accumulation of single-strand DNA gaps during replication [44, 46, 54], among other mechanisms [112]. Here, we show that cells with BER/SSBR defects in XRCC1, APTX, POLB, and LIG3 are sensitive to both the PARPi BMN-673 and the model PARGi PDD00017273 (Figs 4 and 5), supportive of a common mechanism of sensitivity when BER/SSBR is defective. Further, we and others find that PARG inhibitors are synthetically lethal with ATR or CHK1 inhibitors [75, 78], which is also seen with PARP inhibitors [158, 159]. It is reasonable to suggest that defects in BER/SSBR factors, as shown here, lead to elevated strand breaks and the accumulation of single-strand DNA gaps during replication.

PRMT1/PRMT5 inhibitors synergize with PARP inhibitors in HR-proficient cells [80–82, 116], and so we expanded on the enhanced cell killing when combining PARGi and ATRi (Fig. 7). We next evaluated the impact of PARGi response in combination with either a PRMT1 or a PRMT5 inhibitor (Fig. 7). Inhibition of PRMT1 or PRMT5 induces DNA damage and is shown to down-regulate the expression of several DDR genes [116], including suppressing ATR levels and suppressing ATR activation [82], both of which would likely contribute to an enhanced response to PARG inhibition. In support of this hypothesis, we show that there is a strong synergy between PARG inhibitors and PRMT1/PRMT5 inhibitors, albeit to a greater extent in ES-2 cells (Fig. 7).

Collectively, we suggest a model whereby BER/SSBR regulates the accumulation of replication-stress-induced PAR signaling that leads to activation of the S-phase checkpoint, with both the ATR/CHK1 and PRMT1/PRMT5 signaling nodes providing a level of cellular protection. However, when PAR degradation is blocked by PARG inhibition, cells are hypersensitive to further inhibition of the PRMT1/PRMT5/ATR axis (Fig. 7K), highlighting potential biomarkers of PARG inhibitor response that may be explored to enhance the response to this new class of cancer treatments that impact PAR dynamics.

Acknowledgements

The authors would like to thank Drs Abu-Bakr Al-Mehdi, Wito Richter, Aishwarya Prakash, Simon Grelet, Jianfeng Li, Anusha Angajala, and Natalie Gassman, as well as Alison Beiser (University of South Alabama), for suggestions during the initial part of this project. Also, we would like to thank the members of the Sobol Lab at Brown University for helpful data discussions and for keeping the lab supplied (Dan Ivanov), and also thanks to members of the Mani Lab (Brown University) for advice. The purchase and maintenance of the Nikon Ti2-E inverted confocal microscope with Ax-R in our lab at Brown University was provided by generous support from the Dr Robert Browning Foundation.

Author contributions: Md Ibrahim (Data curation [equal], Formal analysis [equal], Investigation [equal], Methodology [equal], Resources [equal], Visualization [equal], Writing—original draft [equal], Writing—review & editing [supporting]), Wynand P. Roos (Data curation [supporting], Formal analysis [supporting], Investigation [lead], Methodology [supporting], Resources [supporting], Validation [supporting], Visualization [supporting], Writing—original draft [supporting], Writing—review & editing [supporting]), Jacob C. Schwartz (Formal analysis [supporting], Investigation [supporting], Writing—review & editing [supporting]), Md Maruf Khan (Formal analysis [supporting], Investigation [supporting], Validation [supporting], Writing—review & editing [supporting]), Rasha Q. Al-Rahahleh (Methodology [supporting], Writing—review & editing [supporting]), Libby A. Beers (Formal analysis [supporting], Investigation [supporting], Writing—review & editing [supporting]), Charlotte R. Pearson (Formal analysis [supporting], Investigation [supporting], Methodology [supporting], Writing—review & editing [supporting]), Kahrie T. Langham (Formal analysis [supporting], Investigation [supporting], Writing—review & editing [supporting]), Louis Boyang (Formal analysis [supporting], Investigation [supporting], Writing—review & editing [supporting]), Jennifer Clark (Formal analysis [supporting], Investigation [supporting], Resources [supporting], Writing—review & editing [supporting]), Faisal Hayat (Resources [supporting]), Qingming Fang (Methodology [supporting], Resources [supporting], Writing—review & editing [supporting]), Christopher A. Koczor (Methodology [supporting], Resources [supporting], Writing—review & editing [supporting]), Marie E. Migaud (Resources [supporting], Supervision [supporting], Writing—review & editing [supporting]), and Robert W. Sobol (Conceptualization [lead], Data curation [equal], Formal analysis [equal], Funding acquisition [equal], Methodology [equal], Project administration [lead], Supervision [lead], Validation [equal], Visualization [equal], Writing—original draft [equal], Writing—review & editing [lead]).

Supplementary data

Supplementary data is available at NAR Cancer online.

Funding

Research in the Sobol lab on DNA repair, the analysis of DNA damage, and the impact of genotoxic exposure & replication stress is funded by grants from the NIH [ES029518, ES028949, CA238061, CA236911, AG069740, and ES032522] and from the NSF [NSF-1841811]. Support was also provided by the Legoretta Cancer Center Endowment Fund (to R.W.S.) and was provided by grants from the Breast Cancer Research Foundation of Alabama, from the Abraham A. Mitchell Distinguished Investigator Fund, from the Mitchell Cancer Institute Molecular & Metabolic Oncology Program Development Fund, and from the Legoretta Cancer Center Endowment Fund (to R.W.S.).

Data availability

The data underlying this article will be shared on reasonable request to the corresponding author.

References

1. Hassa PO, Hottiger MO. The diverse biological roles of mammalian PARPS, a small but powerful family of poly-ADP-ribose polymerases. *Front Biosci* 2008;13:3046–82. https://doi.org/10.2741/2909
2. Saville KM, Clark J, Wilk A *et al.* NAD$^+$-mediated regulation of mammalian base excision repair. *DNA Repair (Amst)* 2020;93:102930. https://doi.org/10.1016/j.dnarep.2020.102930
3. Ueda K, Hayaishi O. ADP-ribosylation. *Annu Rev Biochem* 1985;54:73–100. https://doi.org/10.1146/annurev.bi.54.070185.000445
4. Corda D, Di Girolamo M. Functional aspects of protein mono-ADP-ribosylation. *EMBO J* 2003;22:1953–8. https://doi.org/10.1093/emboj/cdg209
5. Schreiber V, Dantzer F, Ame JC *et al.* Poly(ADP-ribose): novel functions for an old molecule. *Nat Rev Mol Cell Biol* 2006;7:517–28. https://doi.org/10.1038/nrm1963
6. Langelier MF, Mirhasan M, Gilbert K *et al.* PARP enzyme de novo synthesis of protein-free poly(ADP-ribose). *Mol Cell* 2024;84:4758–73. https://doi.org/10.1016/j.molcel.2024.10.024
7. Demeny MA, Virag L. The PARP enzyme family and the hallmarks of cancer part 1. *Cancers* 2021;13:2042.
8. Kratz A, Kim M, Kelly MR *et al.* A multi-scale map of protein assemblies in the DNA damage response. *Cell Syst* 2023;14:447–63.
9. Fouquerel E, Sobol RW. ARTD1 (PARP1) activation and NAD$^+$ in DNA repair and cell death. *DNA Repair (Amst)* 2014;23:27–32. https://doi.org/10.1016/j.dnarep.2014.09.004
10. Fouquerel E, Goellner EM, Yu Z *et al.* ARTD1/PARP1 negatively regulates glycolysis by inhibiting hexokinase 1 independent of NAD$^+$ depletion. *Cell Rep* 2014;8:1819–31. https://doi.org/10.1016/j.celrep.2014.08.036
11. Ahel I, Ahel D, Matsusaka T *et al.* Poly(ADP-ribose)-binding zinc finger motifs in DNA repair/checkpoint proteins. *Nature* 2008;451:81–5. https://doi.org/10.1038/nature06420
12. Liu C, Vyas A, Kassab MA *et al.* The role of poly ADP-ribosylation in the first wave of DNA damage response. *Nucleic Acids Res* 2017;45:8129–41. https://doi.org/10.1093/nar/gkx565
13. Koczor CA, Saville KM, Andrews JF *et al.* Temporal dynamics of base excision/single-strand break repair protein complex assembly/disassembly are modulated by the PARP/NAD$^+$/SIRT6 axis. *Cell Rep* 2021;37:109917. https://doi.org/10.1016/j.celrep.2021.109917
14. Al-Rahahleh RQ, Roos WP, Saville KM *et al.* Overexpression of the WWE domain of RNF146 modulates poly-(ADP)-ribose dynamics at sites of DNA damage. *DNA Repair (Amst)* 2025;150:103845. https://doi.org/10.1016/j.dnarep.2025.103845
15. Al-Rahahleh RQ, Sobol RW. Poly-ADP-ribosylation dynamics, signaling, and analysis. *Environ and Mol Mutagen* 2024;65:315–37. https://doi.org/10.1002/em.22623

16. Liu Y, Kadyrov FA, Modrich P. PARP-1 enhances the mismatch-dependence of 5'-directed excision in human mismatch repair *in vitro*. *DNA Repair (Amst)* 2011;10:1145–53. https://doi.org/10.1016/j.dnarep.2011.08.012
17. Robu M, Shah RG, Petitclerc N *et al.* Role of poly(ADP-ribose) polymerase-1 in the removal of UV-induced DNA lesions by nucleotide excision repair. *Proc Natl Acad Sci USA* 2013;110:1658–63. https://doi.org/10.1073/pnas.1209507110
18. Pines A, Mullenders LH, van Attikum H *et al.* Touching base with PARPs: moonlighting in the repair of UV lesions and double-strand breaks. *Trends Biochem Sci* 2013;38:321–30. https://doi.org/10.1016/j.tibs.2013.03.002
19. Vekariya U, Minakhin L, Chandramouly G *et al.* PARG is essential for Polθ-mediated DNA end-joining by removing repressive poly-ADP-ribose marks. *Nat Commun* 2024;15:5822. https://doi.org/10.1038/s41467-024-50158-7
20. Almeida KH, Sobol RW. A unified view of base excision repair: lesion-dependent protein complexes regulated by post-translational modification. *DNA Repair (Amst)* 2007;6:695–711. https://doi.org/10.1016/j.dnarep.2007.01.009
21. Hanzlikova H, Gittens W, Krejcikova K *et al.* Overlapping roles for PARP1 and PARP2 in the recruitment of endogenous XRCC1 and PNKP into oxidized chromatin. *Nucleic Acids Res* 2017;45:2546–57.
22. Fisher AE, Hochegger H, Takeda S *et al.* Poly(ADP-ribose) polymerase 1 accelerates single-strand break repair in concert with poly(ADP-ribose) glycohydrolase. *Mol Cell Biol* 2007;27:5597–605. https://doi.org/10.1128/MCB.02248-06
23. Almeida KH, Andrews ME, Sobol RW. AP endonuclease 1: biological updates and advances in activity analysis. *Methods Enzymol* 2024;705:347–76.
24. Prasad R, Dyrkheeva N, Williams J *et al.* Mammalian base excision repair: functional partnership between PARP-1 and APE1 in AP-site repair. *PLoS One* 2015;10:e0124269. https://doi.org/10.1371/journal.pone.0124269
25. Sukhanova MV, Khodyreva SN, Lebedeva NA *et al.* Human base excision repair enzymes apurinic/apyrimidinic endonuclease1 (APE1), DNA polymerase beta and poly(ADP-ribose) polymerase 1: interplay between strand-displacement DNA synthesis and proofreading exonuclease activity. *Nucleic Acids Res* 2005;33:1222–9. https://doi.org/10.1093/nar/gki266
26. Soll JM, Sobol RW, Mosammaparast N. Regulation of DNA alkylation damage repair: lessons and therapeutic opportunities. *Trends Biochem Sci* 2017;42:206–18. https://doi.org/10.1016/j.tibs.2016.10.001
27. Svilar D, Goellner EM, Almeida KH *et al.* Base excision repair and lesion-dependent subpathways for repair of oxidative DNA damage. *Antioxid Redox Signaling* 2011;14:2491–507. https://doi.org/10.1089/ars.2010.3466
28. El-Khamisy SF, Masutani M, Suzuki H *et al.* A requirement for PARP-1 for the assembly or stability of XRCC1 nuclear foci at sites of oxidative DNA damage. *Nucleic Acids Res* 2003;31:5526–33. https://doi.org/10.1093/nar/gkg761
29. Campalans A, Kortulewski T, Amouroux R *et al.* Distinct spatiotemporal patterns and PARP dependence of XRCC1 recruitment to single-strand break and base excision repair. *Nucleic Acids Res* 2013;41:3115–29. https://doi.org/10.1093/nar/gkt025
30. Li J, Koczor CA, Saville KM *et al.* Overcoming temozolomide resistance in glioblastoma via enhanced NAD^+ bioavailability and inhibition of poly-ADP-ribose glycohydrolase. *Cancers* 2022;14:3572.
31. Li J, K MS, Ibrahim M *et al.* NAD^+ bioavailability mediates PARG inhibition-induced replication arrest, intra S-phase checkpoint and apoptosis in glioma stem cells. *NAR Cancer* 2021;3:zcab044. https://doi.org/10.1093/narcan/zcab044
32. Kim IK, Stegeman RA, Brosey CA *et al.* A quantitative assay reveals ligand specificity of the DNA scaffold repair protein XRCC1 and efficient disassembly of complexes of XRCC1 and the poly(ADP-ribose) polymerase 1 by poly(ADP-ribose) glycohydrolase. *J Biol Chem* 2015;290:3775–83. https://doi.org/10.1074/jbc.M114.624718
33. Hanahan D, Weinberg RA. Hallmarks of cancer: the next generation. *Cell* 2011;144:646–74. https://doi.org/10.1016/j.cell.2011.02.013
34. Berti M, Cortez D, Lopes M. The plasticity of DNA replication forks in response to clinically relevant genotoxic stress. *Nat Rev Mol Cell Biol* 2020;21:633–51. https://doi.org/10.1038/s41580-020-0257-5
35. Gaillard H, Garcia-Muse T, Aguilera A. Replication stress and cancer. *Nat Rev Cancer* 2015;15:276–89. https://doi.org/10.1038/nrc3916
36. Kim JC, Mirkin SM. The balancing act of DNA repeat expansions. *Curr Opin Genet Dev* 2013;23:280–8. https://doi.org/10.1016/j.gde.2013.04.009
37. Paeschke K, Bochman ML, Garcia PD *et al.* Pif1 family helicases suppress genome instability at G-quadruplex motifs. *Nature* 2013;497:458–62. https://doi.org/10.1038/nature12149
38. Primo LMF, Teixeira LK. DNA replication stress: oncogenes in the spotlight. *Genet Mol Biol* 2019;43:e20190138. https://doi.org/10.1590/1678-4685-gmb-2019-0138
39. Poli J, Tsaponina O, Crabbe L *et al.* dNTP pools determine fork progression and origin usage under replication stress. *EMBO J* 2012;31:883–94. https://doi.org/10.1038/emboj.2011.470
40. Helmrich A, Ballarino M, Tora L. Collisions between replication and transcription complexes cause common fragile site instability at the longest human genes. *Mol Cell* 2011;44:966–77. https://doi.org/10.1016/j.molcel.2011.10.013
41. Promonet A, Padioleau I, Liu Y *et al.* Topoisomerase 1 prevents replication stress at R-loop-enriched transcription termination sites. *Nat Commun* 2020;11:3940. https://doi.org/10.1038/s41467-020-17858-2
42. Zheng L, Shen B. Okazaki fragment maturation: nucleases take centre stage. *J Mol Cell Biol* 2011;3:23–30. https://doi.org/10.1093/jmcb/mjq048
43. Panzarino NJ, Krais JJ, Cong K *et al.* Replication gaps underlie BRCA deficiency and therapy response. *Cancer Res* 2021;81:1388–97. https://doi.org/10.1158/0008-5472.CAN-20-1602
44. Cong K, Peng M, Kousholt AN *et al.* Replication gaps are a key determinant of PARP inhibitor synthetic lethality with BRCA deficiency. *Mol Cell* 2021;81:3128–44. https://doi.org/10.1016/j.molcel.2021.07.015
45. Bai YR, Yang WG, Jia R *et al.* The recent advance and prospect of poly(ADP-ribose) polymerase inhibitors for the treatment of cancer. *Med Res Rev* 2025;45:214–73. https://doi.org/10.1002/med.22069
46. Ravindranathan R, Somuncu O, da Costa A *et al.* PARG inhibitor sensitivity correlates with accumulation of single-stranded DNA gaps in preclinical models of ovarian cancer. *Proc Natl Acad Sci USA* 2024;121:e2413954121. https://doi.org/10.1073/pnas.2413954121
47. Liu Z, Jiang H, Lee SY *et al.* FANCM promotes PARP inhibitor resistance by minimizing ssDNA gap formation and counteracting resection inhibition. *Cell Rep* 2024;43:114464. https://doi.org/10.1016/j.celrep.2024.114464
48. Gralewska P, Gajek A, Rybaczek D *et al.* The influence of PARP, ATR, CHK1 inhibitors on premature mitotic entry and genomic instability in high-grade serous BRCA(MUT) and BRCA(WT) ovarian cancer cells. *Cells* 2022;11:1889. https://doi.org/10.3390/cells11121889 .
49. Hewitt G, Borel V, Segura-Bayona S *et al.* Defective ALC1 nucleosome remodeling confers PARPi sensitization and synthetic lethality with HRD. *Mol Cell* 2021;81:767–83. https://doi.org/10.1016/j.molcel.2020.12.006
50. Slade D. PARP and PARG inhibitors in cancer treatment. *Genes Dev* 2020;34:360–94. https://doi.org/10.1101/gad.334516.119

51. Ronson GE, Piberger AL, Higgs MR *et al.* PARP1 and PARP2 stabilise replication forks at base excision repair intermediates through Fbh1-dependent Rad51 regulation. *Nat Commun* 2018;9:746. https://doi.org/10.1038/s41467-018-03159-2
52. D'Andrea AD. Mechanisms of PARP inhibitor sensitivity and resistance. *DNA Repair (Amst)* 2018;71:172–6. https://doi.org/10.1016/j.dnarep.2018.08.021
53. Carruthers RD, Ahmed SU, Ramachandran S *et al.* Replication stress drives constitutive activation of the DNA damage response and radioresistance in glioblastoma stem-like cells. *Cancer Res* 2018;78:5060–71. https://doi.org/10.1158/0008-5472.CAN-18-0569
54. Ray Chaudhuri A, Ahuja AK, Herrador R *et al.* Poly(ADP-ribosyl) glycohydrolase prevents the accumulation of unusual replication structures during unperturbed S phase. *Mol Cell Biol* 2015;35:856–65. https://doi.org/10.1128/MCB.01077-14
55. Illuzzi G, Fouquerel E, Ame JC *et al.* PARG is dispensable for recovery from transient replicative stress but required to prevent detrimental accumulation of poly(ADP-ribose) upon prolonged replicative stress. *Nucleic Acids Res* 2014;42:7776–92. https://doi.org/10.1093/nar/gku505
56. Min W, Bruhn C, Grigaravicius P *et al.* Poly(ADP-ribose) binding to Chk1 at stalled replication forks is required for S-phase checkpoint activation. *Nat Commun* 2013;4:2993. https://doi.org/10.1038/ncomms3993
57. Ortega P, Bournique E, Li J *et al.* Mechanism of DNA replication fork breakage and PARP1 hyperactivation during replication catastrophe. *Sci Adv* 2025;11:eadu0437. https://doi.org/10.1126/sciadv.adu0437
58. Laspata N, Kaur P, Mersaoui SY *et al.* PARP1 associates with R-loops to promote their resolution and genome stability. *Nucleic Acids Res* 2023;51:2215–37. https://doi.org/10.1093/nar/gkad066
59. Schreuder A, Wendel TJ, Dorresteijn CGV *et al.* (Single-stranded DNA) gaps in understanding BRCAness. *Trends Genet* 2024;40:757–71. https://doi.org/10.1016/j.tig.2024.04.013
60. Tirman S, Quinet A, Wood M *et al.* Temporally distinct post-replicative repair mechanisms fill PRIMPOL-dependent ssDNA gaps in human cells. *Mol Cell* 2021;81:4026–40. https://doi.org/10.1016/j.molcel.2021.09.013
61. Wondisford AR, Lee J, Lu R *et al.* Deregulated DNA ADP-ribosylation impairs telomere replication. *Nat Struct Mol Biol* 2024;31:791–800. https://doi.org/10.1038/s41594-024-01279-6
62. De Rosa M, Barnes RP, Nyalapatla PR *et al.* OGG1 and MUTYH repair activities promote telomeric 8-oxoguanine induced senescence in human fibroblasts. *Nature communications* 2025;16:893. https://doi.org/10.1038/s41467-024-55638-4
63. Salvati E, Scarsella M, Porru M *et al.* PARP1 is activated at telomeres upon G4 stabilization: possible target for telomere-based therapy. *Oncogene* 2010;29:6280–93. https://doi.org/10.1038/onc.2010.344
64. Gaur P, Bain FE, Meah R *et al.* Single-molecule analysis of PARP1-G-quadruplex interaction. bioRxiv, https://doi.org/10.1101/2025.01.06.631587, 8 January 2025, preprint: not peer reviewed.
65. Edwards AD, Marecki JC, Byrd AK *et al.* G-quadruplex loops regulate PARP-1 enzymatic activation. *Nucleic Acids Res* 2021;49:416–31. https://doi.org/10.1093/nar/gkaa1172
66. Zimmermann M, Murina O, Reijns MAM *et al.* CRISPR screens identify genomic ribonucleotides as a source of PARP-trapping lesions. *Nature* 2018;559:285–9. https://doi.org/10.1038/s41586-018-0291-z
67. Hanzlikova H, Kalasova I, Demin AA *et al.* The importance of poly(ADP-Ribose) polymerase as a sensor of unligated Okazaki fragments during DNA replication. *Mol Cell* 2018;71:319–31. https://doi.org/10.1016/j.molcel.2018.06.004
68. Bryant HE, Schultz N, Thomas HD *et al.* Specific killing of BRCA2-deficient tumours with inhibitors of poly(ADP-ribose) polymerase. *Nature* 2005;434:913–7. https://doi.org/10.1038/nature03443
69. Farmer H, McCabe N, Lord CJ *et al.* Targeting the DNA repair defect in BRCA mutant cells as a therapeutic strategy. *Nature* 2005;434:917–21. https://doi.org/10.1038/nature03445
70. Mortusewicz O, Fouquerel E, Ame JC *et al.* PARG is recruited to DNA damage sites through poly(ADP-ribose)- and PCNA-dependent mechanisms. *Nucleic Acids Res* 2011;39:5045–56. https://doi.org/10.1093/nar/gkr099
71. Kaufmann T, Grishkovskaya I, Polyansky AA *et al.* A novel non-canonical PIP-box mediates PARG interaction with PCNA. *Nucleic Acids Res* 2017;45:9741–59. https://doi.org/10.1093/nar/gkx604
72. Houl JH, Ye Z, Brosey CA *et al.* Selective small molecule PARG inhibitor causes replication fork stalling and cancer cell death. *Nat Commun* 2019;10:5654. https://doi.org/10.1038/s41467-019-13508-4
73. Pillay N, Brady RM, Dey M *et al.* DNA replication stress and emerging prospects for PARG inhibitors in ovarian cancer therapy. *Prog Biophys Mol Biol* 2021;163:160–70. https://doi.org/10.1016/j.pbiomolbio.2021.01.004
74. Pillay N, Tighe A, Nelson L *et al.* DNA replication vulnerabilities render ovarian cancer cells sensitive to poly(ADP-Ribose) glycohydrolase inhibitors. *Cancer Cell* 2019;35:519–33. https://doi.org/10.1016/j.ccell.2019.02.004
75. Khan MM, Roos WP, Pearson CR *et al.* DNA polymerase beta expression in head & neck cancer modulates the poly(ADP-ribose)-mediated replication checkpoint. *DNA Repair (Amst)* 2025;150:103853. https://doi.org/10.1016/j.dnarep.2025.103853
76. Coulson-Gilmer C, Morgan RD, Nelson L *et al.* Replication catastrophe is responsible for intrinsic PAR glycohydrolase inhibitor-sensitivity in patient-derived ovarian cancer models. *J Exp Clin Cancer Res* 2021;40:323. https://doi.org/10.1186/s13046-021-02124-0
77. Saville KM, Al-Rahahleh RQ, Siddiqui AH *et al.* Oncometabolite 2-hydroxyglutarate suppresses basal protein levels of DNA polymerase beta that enhances alkylating agent and PARG inhibition induced cytotoxicity. *DNA Repair (Amst)* 2024;140:103700. https://doi.org/10.1016/j.dnarep.2024.103700
78. Acharya G, Mani C, Sah N *et al.* CHK1 inhibitor induced PARylation by targeting PARG causes excessive replication and metabolic stress and overcomes chemoresistance in ovarian cancer. *Cell Death Discov* 2024;10:278. https://doi.org/10.1038/s41420-024-02040-0
79. Hwang JW, Cho Y, Bae GU *et al.* Protein arginine methyltransferases: promising targets for cancer therapy. *Exp Mol Med* 2021;53:788–808. https://doi.org/10.1038/s12276-021-00613-y
80. Zhang Y, Xu M, Yuan J *et al.* Repression of PRMT activities sensitize homologous recombination-proficient ovarian and breast cancer cells to PARP inhibitor treatment. bioRxiv, https://doi.org/10.1101/2024.05.21.595159, 29 April 2025, preprint: not peer reviewed.
81. O'Brien S, Butticello M, Thompson C *et al.* Inhibiting PRMT5 induces DNA damage and increases anti-proliferative activity of Niraparib, a PARP inhibitor, in models of breast and ovarian cancer. *BMC Cancer* 2023;23:775. https://doi.org/10.1186/s12885-023-11260-z
82. Li Y, Dobrolecki LE, Sallas C *et al.* PRMT blockade induces defective DNA replication stress response and synergizes with PARP inhibition. *Cell Reports Medicine* 2023;4:101326. https://doi.org/10.1016/j.xcrm.2023.101326
83. Giroud-Gerbetant J, Joffraud M, Giner MP *et al.* A reduced form of nicotinamide riboside defines a new path for NAD^+ biosynthesis and acts as an orally bioavailable NAD^+ precursor.

Molecular Metabolism 2019;30:192–202. https://doi.org/10.1016/j.molmet.2019.09.013
84. Tang JB, Svilar D, Trivedi RN *et al.* N-methylpurine DNA glycosylase and DNA polymerase β modulate BER inhibitor potentiation of glioma cells to temozolomide. *Neuro Oncol* 2011;13:471–86. https://doi.org/10.1093/neuonc/nor011
85. Guillemette S, Serra RW, Peng M *et al.* Resistance to therapy in BRCA2 mutant cells due to loss of the nucleosome remodeling factor CHD4. *Genes Dev* 2015;29:489–94. https://doi.org/10.1101/gad.256214.114
86. Sakai W, Swisher EM, Jacquemont C *et al.* Functional restoration of BRCA2 protein by secondary BRCA2 mutations in BRCA2-mutated ovarian carcinoma. *Cancer Res* 2009;69:6381–6. https://doi.org/10.1158/0008-5472.CAN-09-1178
87. Bodnar AG, Ouellette M, Frolkis M *et al.* Extension of life-span by introduction of telomerase into normal human cells. *Science* 1998;279:349–52. https://doi.org/10.1126/science.279.5349.349
88. Slyskova J, Sabatella M, Ribeiro-Silva C *et al.* Base and nucleotide excision repair facilitate resolution of platinum drugs-induced transcription blockage. *Nucleic Acids Res* 2018;46:9537–49. https://doi.org/10.1093/nar/gky764
89. Fang Q, Inanc B, Schamus S *et al.* HSP90 regulates DNA repair via the interaction between XRCC1 and DNA polymerase beta. *Nat Commun* 2014;5:5513. https://doi.org/10.1038/ncomms6513
90. Desjardins P, Hansen JB, Allen M. Microvolume protein concentration determination using the NanoDrop 2000c spectrophotometer. *J Vis Exp* 2009;e1610. https://doi.org/10.3791/1610
91. Chen G, Deng X. Cell synchronization by double thymidine block. *Bio Protoc* 2018;8:e2994. https://doi.org/10.21769/BioProtoc.2994
92. Chen M, Huang J, Yang X *et al.* Serum starvation induced cell cycle synchronization facilitates human somatic cells reprogramming. *PLoS One* 2012;7:e28203. https://doi.org/10.1371/journal.pone.0028203
93. VanArsdale T, Boshoff C, Arndt KT *et al.* Molecular pathways: targeting the cyclin D-CDK4/6 axis for cancer treatment. *Clin Cancer Res* 2015;21:2905–10. https://doi.org/10.1158/1078-0432.CCR-14-0816
94. Inanc B, Fang Q, Roos WP *et al.* TRIP12's role in the governance of DNA polymerase beta involvement in DNA damage response and repair. *Nucleic Acids Res* 2025;53:gkaf574. https://doi.org/10.1093/nar/gkaf574
95. Kessel S, Cribbes S, Bonasu S *et al.* Real-time apoptosis and viability high-throughput screening of 3D multicellular tumor spheroids using the Celigo image cytometer. *SLAS Discovery* 2018;23:202–10. https://doi.org/10.1177/2472555217731076
96. Cho KF, Branon TC, Udeshi ND *et al.* Proximity labeling in mammalian cells with TurboID and split-TurboID. *Nat Protoc* 2020;15:3971–99. https://doi.org/10.1038/s41596-020-0399-0
97. Liu Q, Yin X, Languino LR *et al.* Evaluation of drug combination effect using a Bliss independence dose-response surface model. *Stat Biopharm Res* 2018;10:112–22. https://doi.org/10.1080/19466315.2018.1437071
98. Kutuzov MM, Belousova EA, Kurgina TA *et al.* The contribution of PARP1, PARP2 and poly(ADP-ribosyl)ation to base excision repair in the nucleosomal context. *Sci Rep* 2021;11:4849. https://doi.org/10.1038/s41598-021-84351-1
99. Guerrero Llobet S, Bhattacharya A, Everts M *et al.* An mRNA expression-based signature for oncogene-induced replication-stress. *Oncogene* 2022;41:1216–24. https://doi.org/10.1038/s41388-021-02162-0
100. da Costa A, Chowdhury D, Shapiro GI *et al.* Targeting replication stress in cancer therapy. *Nat Rev Drug Discov* 2023;22:38–58. https://doi.org/10.1038/s41573-022-00558-5
101. Weller M, Rieger J, Grimmel C *et al.* Predicting chemoresistance in human malignant glioma cells: the role of molecular genetic analyses. *Int J Cancer* 1998;79:640–4. https://doi.org/10.1002/(SICI)1097-0215(19981218)79:6⟨640::AID-IJC15⟩3.0.CO;2-Z
102. Flaman JM, Frebourg T, Moreau V *et al.* A simple p53 functional assay for screening cell lines, blood, and tumors. *Proc Natl Acad Sci USA* 1995;92:3963–7. https://doi.org/10.1073/pnas.92.9.3963
103. Ishii N, Maier D, Merlo A *et al.* Frequent co-alterations of TP53, p16/CDKN2A, p14ARF, PTEN tumor suppressor genes in human glioma cell lines. *Brain Pathol* 1999;9:469–79. https://doi.org/10.1111/j.1750-3639.1999.tb00536.x
104. Wischhusen J, Naumann U, Ohgaki H *et al.* CP-31398, a novel p53-stabilizing agent, induces p53-dependent and p53-independent glioma cell death. *Oncogene* 2003;22:8233–45. https://doi.org/10.1038/sj.onc.1207198
105. Gorgoulis VG, Vassiliou LV, Karakaidos P *et al.* Activation of the DNA damage checkpoint and genomic instability in human precancerous lesions. *Nature* 2005;434:907–13. https://doi.org/10.1038/nature03485
106. Guo C, Guo L, Peng C *et al.* p53-driven replication stress in nucleoli of malignant epithelial ovarian cancer. *Exp Cell Res* 2022;417:113225. https://doi.org/10.1016/j.yexcr.2022.113225
107. Bryant HE, Petermann E, Schultz N *et al.* PARP is activated at stalled forks to mediate Mre11-dependent replication restart and recombination. *EMBO J* 2009;28:2601–15. https://doi.org/10.1038/emboj.2009.206
108. Chen Q, Kassab MA, Dantzer F *et al.* PARP2 mediates branched poly ADP-ribosylation in response to DNA damage. *Nat Commun* 2018;9:3233. https://doi.org/10.1038/s41467-018-05588-5
109. Cho KF, Branon TC, Rajeev S *et al.* Split-TurboID enables contact-dependent proximity labeling in cells. *Proc Natl Acad Sci USA* 2020;117:12143–54. https://doi.org/10.1073/pnas.1919528117
110. Demin AA, Hirota K, Tsuda M *et al.* XRCC1 prevents toxic PARP1 trapping during DNA base excision repair. *Mol Cell* 2021;81:3018–30. https://doi.org/10.1016/j.molcel.2021.05.009
111. Serrano-Benitez A, Wells SE, Drummond-Clarke L *et al.* Unrepaired base excision repair intermediates in template DNA strands trigger replication fork collapse and PARP inhibitor sensitivity. *EMBO J* 2023;42:e113190. https://doi.org/10.15252/embj.2022113190
112. Jackson LM, Moldovan GL. Mechanisms of PARP1 inhibitor resistance and their implications for cancer treatment. *NAR Cancer* 2022;4:zcac042. https://doi.org/10.1093/narcan/zcac042
113. Murai J, Huang SY, Das BB *et al.* Trapping of PARP1 and PARP2 by clinical PARP inhibitors. *Cancer Res* 2012;72:5588–99. https://doi.org/10.1158/0008-5472.CAN-12-2753
114. Murai J, Huang SY, Renaud A *et al.* Stereospecific PARP trapping by BMN 673 and comparison with olaparib and rucaparib. *Mol Cancer Ther* 2014;13:433–43. https://doi.org/10.1158/1535-7163.MCT-13-0803
115. Dunlop CR, Wallez Y, Johnson TI *et al.* Complete loss of ATM function augments replication catastrophe induced by ATR inhibition and gemcitabine in pancreatic cancer models. *Br J Cancer* 2020;123:1424–36. https://doi.org/10.1038/s41416-020-1016-2
116. Carter J, Hulse M, Sivakumar M *et al.* PRMT5 inhibitors regulate DNA damage repair pathways in cancer cells and improve response to PARP inhibition and chemotherapies. *Cancer Res Commun* 2023;3:2233–43. https://doi.org/10.1158/2767-9764.CRC-23-0070
117. Bliss H, Bouley RA, Petreaca RC. Regulation of DNA repair gene expression by PRMT5. *MicroPubl Biol* 2025;2025:10.17912/micropub.biology.001631.
118. Onishi S, Jayamohan S, Chowdhury A *et al.* PRMT5 inhibition sensitizes glioblastoma tumor models to temozolomide. *Research Square* 2025. https://doi.org/10.21203/rs.3.rs-5936706/v1

119. Gillespie MS, Chiang K, Regan-Mochrie GL *et al.* PRMT5-regulated splicing of DNA repair genes drives chemoresistance in breast cancer stem cells. *Oncogene* 2025;44:862–76. https://doi.org/10.1038/s41388-024-03264-1
120. Pandya P, Vendetti FP, El-Ghoubaira J *et al.* Deoxyuridine-rich cytoplasmic DNA antagonizes STING-dependent innate immune responses and sensitizes resistant tumors to anti-PD-L1 therapy. bioRxiv, https://doi.org/10.1101/2024.04.04.588079, 5 April 2024, preprint: not peer reviewed.
121. Saxena S, Nabel CS, Seay TW *et al.* Unprocessed genomic uracil as a source of DNA replication stress in cancer cells. *Mol Cell* 2024;84:2036–52. https://doi.org/10.1016/j.molcel.2024.04.004
122. Vens C, Sobol RW. In: Johnson DE (ed.), *Cell death signaling in cancer biology and treatment. X.-M. Yin and Z. Dong (Series eds.), Cell Death in Biology and Diseases*. New York: Springer, 2013.
123. Hoeijmakers JH. Genome maintenance mechanisms for preventing cancer. *Nature* 2001;411:366–74. https://doi.org/10.1038/35077232
124. Trucco C, Oliver FJ, de Murcia G *et al.* DNA repair defect in poly(ADP-ribose) polymerase-deficient cell lines. *Nucleic Acids Res* 1998;26:2644–9. https://doi.org/10.1093/nar/26.11.2644
125. Ame JC, Rolli V, Schreiber V *et al.* PARP-2, a novel mammalian DNA damage-dependent poly(ADP-ribose) polymerase. *J Biol Chem* 1999;274:17860–8. https://doi.org/10.1074/jbc.274.25.17860
126. Zhang H, Zha S. The dynamics and regulation of PARP1 and PARP2 in response to DNA damage and during replication. *DNA Repair (Amst)* 2024;140:103690. https://doi.org/10.1016/j.dnarep.2024.103690
127. Hassa PO, Haenni SS, Elser M *et al.* Nuclear ADP-ribosylation reactions in mammalian cells: where are we today and where are we going? *Microbiol Mol Biol Rev* 2006;70:789–829. https://doi.org/10.1128/MMBR.00040-05
128. Vendetti FP, Pandya P, Sclafani CR *et al.* Uracil-DNA glycosylase deficiency is associated with repressed tumor cell-intrinsic inflammatory signaling and altered sensitivity to exogenous interferons. bioRxiv, https://doi.org/10.1101/2025.07.28.666960, 1 August 2025, preprint: not peer reviewed.
129. Musiani D, Yucel H, Vallette M *et al.* Uracil processing by SMUG1 in the absence of UNG triggers homologous recombination and selectively kills BRCA1/2-deficient tumors. *Mol Cell* 2025;85:1072–84. https://doi.org/10.1016/j.molcel.2025.01.031
130. Mosler T, Baymaz HI, Graf JF *et al.* PARP1 proximity proteomics reveals interaction partners at stressed replication forks. *Nucleic Acids Res* 2022;50:11600–18. https://doi.org/10.1093/nar/gkac948
131. Petropoulos M, Karamichali A, Rossetti GG *et al.* Transcription-replication conflicts underlie sensitivity to PARP inhibitors. *Nature* 2024;628:433–41. https://doi.org/10.1038/s41586-024-07217-2
132. Simbulan-Rosenthal CM, Rosenthal DS, Boulares AH *et al.* Regulation of the expression or recruitment of components of the DNA synthesome by poly(ADP-ribose) polymerase. *Biochemistry* 1998;37:9363–70. https://doi.org/10.1021/bi9731089
133. Simbulan-Rosenthal CM, Rosenthal DS, Iyer S *et al.* Involvement of PARP and poly(ADP-ribosyl)ation in the early stages of apoptosis and DNA replication. *Mol Cell Biochem* 1999;193:137–48. https://doi.org/10.1023/A:1006988832729
134. Dantzer F, Nasheuer HP, Vonesch JL *et al.* Functional association of poly(ADP-ribose) polymerase with DNA polymerase alpha-primase complex: a link between DNA strand break detection and DNA replication. *Nucleic Acids Res* 1998;26:1891–8. https://doi.org/10.1093/nar/26.8.1891
135. Berti M, Ray Chaudhuri A, Thangavel S *et al.* Human RECQ1 promotes restart of replication forks reversed by DNA topoisomerase I inhibition. *Nat Struct Mol Biol* 2013;20:347–54. https://doi.org/10.1038/nsmb.2501
136. Xie S, Mortusewicz O, Ma HT *et al.* Timeless interacts with PARP-1 to promote homologous recombination repair. *Mol Cell* 2015;60:163–76. https://doi.org/10.1016/j.molcel.2015.07.031
137. Schreiber V, Ame JC, Dolle P *et al.* Poly(ADP-ribose) polymerase-2 (PARP-2) is required for efficient base excision DNA repair in association with PARP-1 and XRCC1. *J Biol Chem* 2002;277:23028–36. https://doi.org/10.1074/jbc.M202390200
138. Koczor CA, Haider AJ, Saville KM *et al.* Live cell detection of poly(ADP-Ribose) for use in genetic and genotoxic compound screens. *Cancers* 2022;14:3676. https://doi.org/10.3390/cancers14153676 .
139. Call N, Tomkinson AE. Joining of DNA breaks- interplay between DNA ligases and poly (ADP-ribose) polymerases. *DNA Repair (Amst)* 2025;149:103843. https://doi.org/10.1016/j.dnarep.2025.103843
140. Kao HI, Bambara RA. The protein components and mechanism of eukaryotic Okazaki fragment maturation. *Crit Rev Biochem Mol Biol* 2003;38:433–52. https://doi.org/10.1080/10409230390259382
141. Kumamoto S, Nishiyama A, Chiba Y *et al.* HPF1-dependent PARP activation promotes LIG3-XRCC1-mediated backup pathway of Okazaki fragment ligation. *Nucleic Acids Res* 2021;49:5003–16. https://doi.org/10.1093/nar/gkab269
142. Gottipati P, Vischioni B, Schultz N *et al.* Poly(ADP-ribose) polymerase is hyperactivated in homologous recombination-defective cells. *Cancer Res* 2010;70:5389–98. https://doi.org/10.1158/0008-5472.CAN-09-4716
143. Koczor CA, Saville KM, Al-Rahahleh RQ *et al.* Quantitative analysis of nuclear poly(ADP-Ribose) dynamics in response to laser-induced DNA damage. *Methods Mol Biol* 2023;2609:43–59.
144. Fugger K, Bajrami I, Silva Dos Santos M *et al.* Targeting the nucleotide salvage factor DNPH1 sensitizes BRCA-deficient cells to PARP inhibitors. *Science* 2021;372:156–65. https://doi.org/10.1126/science.abb4542
145. Paes Dias M, Tripathi V, van der Heijden I *et al.* Loss of nuclear DNA ligase III reverts PARP inhibitor resistance in BRCA1/53BP1 double-deficient cells by exposing ssDNA gaps. *Mol Cell* 2021;81:4692–708.e9. https://doi.org/10.1016/j.molcel.2021.09.005
146. Goel K, Venkatappa V, Krieger KL *et al.* PARP inhibitor response is enhanced in prostate cancer when XRCC1 expression is reduced. *NAR Cancer* 2025;7:zcaf015. https://doi.org/10.1093/narcan/zcaf015
147. Simpson D, Ling J, Jing Y *et al.* Mapping the genetic interaction network of PARP inhibitor response. bioRxiv, https://doi.org/10.1101/2023.08.19.553986, 20 August 2023, preprint: not peer reviewed.
148. Lazarides K, Engel JL, Meseonznik M *et al.* CRISPR screens identify POLB as a synthetic lethal enhancer of PARP inhibition exclusively in BRCA-mutated tumors. *Mol Cancer Ther* 2025;24:1466–79. https://doi.org/10.1158/1535-7163.MCT-24-0822
149. Koh DW, Lawler AM, Poitras MF *et al.* Failure to degrade poly(ADP-ribose) causes increased sensitivity to cytotoxicity and early embryonic lethality. *Proc Natl Acad Sci USA* 2004;101:17699–704. https://doi.org/10.1073/pnas.0406182101
150. Nie L, Wang C, Huang M *et al.* DePARylation is critical for S phase progression and cell survival. *eLife* 2024;12:RP89303. https://doi.org/10.7554/eLife.89303
151. Tentori L, Leonetti C, Scarsella M *et al.* Poly(ADP-ribose) glycohydrolase inhibitor as chemosensitiser of malignant melanoma for temozolomide. *Eur J Cancer* 2005;41:2948–57. https://doi.org/10.1016/j.ejca.2005.08.027
152. Fathers C, Drayton RM, Solovieva S *et al.* Inhibition of poly(ADP-ribose) glycohydrolase (PARG) specifically kills

BRCA2-deficient tumor cells. *Cell Cycle* 2012;11:990–7. https://doi.org/10.4161/cc.11.5.19482
153. Andronikou C, Burdova K, Dibitetto D *et al.* PARG-deficient tumor cells have an increased dependence on EXO1/FEN1-mediated DNA repair. *EMBO J* 2024;43:1015–42. https://doi.org/10.1038/s44318-024-00043-2
154. Sugitani N, Vendetti FP, Cipriano AJ *et al.* Thymidine rescues ATR kinase inhibitor-induced deoxyuridine contamination in genomic DNA, cell death, and interferon-α/β expression. *Cell Rep* 2022;40:111371. https://doi.org/10.1016/j.celrep.2022.111371
155. Randolph K, Hyder U, D'Orso I. KAP1/TRIM28: transcriptional activator and/or repressor of viral and cellular programs? *Front Cell Infect Microbiol* 2022;12:834636. https://doi.org/10.3389/fcimb.2022.834636
156. Blasius M, Forment JV, Thakkar N *et al.* A phospho-proteomic screen identifies substrates of the checkpoint kinase Chk1. *Genome Biol* 2011;12:R78. https://doi.org/10.1186/gb-2011-12-8-r78
157. Ziv Y, Bielopolski D, Galanty Y *et al.* Chromatin relaxation in response to DNA double-strand breaks is modulated by a novel ATM- and KAP-1 dependent pathway. *Nat Cell Biol* 2006;8:870–6. https://doi.org/10.1038/ncb1446
158. McCabe N, Turner NC, Lord CJ *et al.* Deficiency in the repair of DNA damage by homologous recombination and sensitivity to poly(ADP-ribose) polymerase inhibition. *Cancer Res* 2006;66:8109–15. https://doi.org/10.1158/0008-5472.CAN-06-0140
159. Mitchell C, Park M, Eulitt P *et al.* Poly(ADP-ribose) polymerase 1 modulates the lethality of CHK1 inhibitors in carcinoma cells. *Mol Pharmacol* 2010;78:909–17. https://doi.org/10.1124/mol.110.067199

Received: August 19, 2025. **Revised:** December 10, 2025. **Accepted:** December 10, 2025